










The bauxite-bearing lateritic profile of the Jequié Complex, São Francisco Craton, Brazil: potential for rare earth elements mineralization and insights on the mineral system

Daniel Augusto de Miranda^{1*} , Caroline Couto Santos¹ , Fabrício Pereira dos Santos¹ , Anderson Roque Araújo dos Santos Meneses¹ , Carlos Magno Santos Clemente^{2,3} , Rita Cunha Leal Menezes de Oliveira¹ , Isabel Leonor Iza Echeverria Herrera⁴ 

¹Geological Survey of Brazil – CPRM, Avenida Ulysses Guimarães, 2862, Sussuarana, Centro Administrativo da Bahia, Salvador-BA, Brazil, CEP 41213-000

²University Center UniFG, Avenida Pedro Felipe Duarte, 4911, São Sebastião, Guanambi-BA, Brazil, CEP 46430-000

³Present address: Federal Institute of the Northern of Minas Gerais - IFNMG, Rodovia MG-404, Km 02, s/n, Zona Rural, Salinas-MG, Brazil, CEP 39560-000

⁴Federal University of Rondônia, BR-364, km 9,5, Porto Velho-RO, Brazil, CEP 76801-059

Abstract

The Jequié Block is located at the northeastern portion of the São Francisco Craton and represents the Archean tectonic paleoplate that hosts the Jequié Complex. The rocks of the Jequié Complex are cogenetic, enderbritic-charnockitic plutons, which were intruded by gabbros, norites and anorthosites, and subsequently all these rocks were re-equilibrated in granulite facies. Three bauxite occurrences were mapped at the southeastern portion of the Jequié Block, named Itaji (ITJ), Casa de Farinha (CDF) and Valentim (VLT), which are hosted by the bedrock of the units Poço Preto and Santa Inês – Volta do Rio. The Poço Preto Unit is composed of granulitic granodiorites to tonalities, while Santa Inês – Volta do Rio is composed of granulitic granites to granodiorites. The stream sediment results highlighted good geographic correlation between the content of Al, Fe, REE+Y+Sc and Ce in the catchments at the mineralized area. On the ITJ, the vertical profile indicates a lateritic sequence composed of the bedrock (i), saprock (ii), saprolite (iii) and pedolith (iv), while the upper part is the lateritic duricrust (v). The results of petrography, X-ray powder diffraction and whole rock geochemistry, supports the lateritic evolution. This vertical profile was later redeposited through surficial process in a proximal place. The breakdown of K-feldspar and plagioclase into kaolinite started at the weathering front and was continuously intensified towards the saprolite, as well as the transformation of the biotite and amphibole into goethite. The halloysite was identified as an intermediate mineral between the K-feldspar and kaolinite. The kaolinite locally was represented by its polymorph dickite. The transformation of the kaolinite into gibbsite happened between the saprolite and the pedolith, the main reaction in terms of the mineralization was the pseudomorphic feldspar replacement by gibbsite. The presence of the nordstrandite at CDF could be related to local conditions of the weathering, and/or to the bedrock geochemical composition in the region.

Article Information

Publication type: Research Papers
Received 4 January 2023
Accepted 19 April 2023
Online pub. 5 May 2023
Editor: Carlos Spier

Keywords:

Weathering
parent rock
X-ray powder diffraction
gibbsite

*Corresponding author

Daniel Augusto de Miranda
E-mail address: daniel.miranda@sgb.gov.br

1. Introduction

The Brazilian Federal Government released a list with the strategic minerals to the Brazilian economy, and both aluminum ore and the rare earth elements are stated therein Oliveira (2021). The bauxites are the main raw material of the aluminum industry, which are rocks composed of aluminum hydroxide minerals (Retallack 2010). The Brazil has eleven bauxite mines under operation and the largest productions are placed in the Amazon region (Costa 2016). The laterite (or residual) ores, including bauxite, are among the most relevant

non-conventional deposits for the production of REE (Wang et al. 2011). There are no mines currently exploiting REE in Brazil, and the most advanced research projects are targeting REE mineralization hosted by carbonatite complexes, such those from Alto do Paranaíba Igneous Province (Takehara et al. 2015).

During the first decade of the 2000's, the Rio Tinto mining company developed the Amargosa Bauxite Project, currently with limited activity, targeting gibbsite mineralization in the regolith of the Jequié Complex granulites (Costa 2016; Stausholm 2021). Fernandes (1996 and references therein)



assessed the REE potential at the Jequié Complex rocks and Santos Junior (2019) argued in favor of residual-type ion adsorption deposit (Balaram 2019) to explain the REE mineralization in the regolith. Fernandes et al. (2019) identified minerals of the chevkinite group in the bedrock as one of the possible REE-bearing parent minerals.

The Jequié Block (Barbosa and Sabaté 2002), which is the Archean tectonic paleoplate that hosts the rocks of the Jequié Complex (Barbosa 1990), is currently under investigation by the Contendas-Macajuba Project (CMP). The CMP is located in the central-eastern portion of the Bahia state (Figure 1A). During geological mapping, three bauxite occurrences were identified, here named Itaji (ITJ), Casa de Farinha (CDF) and Valentim (VLT), and in the following sections we will present the results of the research performed in these occurrences.

2. Geotectonic setting

2.1. Regional geology

The Jequié Block is located in the northeastern portion of the São Francisco Craton, Mantiqueira Province (Almeida 1977, Figure 1B). It is characterized by Archean granulitic migmatites with supracrustal inclusions and several charnockitic intrusions (Barbosa and Sabaté 2002). Both western and eastern border of the Jequié Block are in tectonic contact with the adjacent geotectonic units (Figure 1C), which are represented respectively by the Gavião Block (Barbosa and Sabaté 2002) and Contendas-Mirante volcano-sedimentary belt (Marinho et al. 1995) on the west, and by the Itabuna-Salvador-Curaçá Orogen (Barbosa and Sabaté 2004) on the east.

The studied area is located in the southeastern portion of the Jequié Block. In this region, the rocks of the Jequié Complex are cogenetic, enderbite-charnockite plutons, which were intruded by gabbros, norites and anorthosites, and subsequently all these rocks were re-equilibrated in granulite facies (Barbosa 1990). Fernandes et al. (2019) dated these rock associations and indicated U-Pb ages between 2.6 Ga and 2.5 Ga. They also showed that these rocks have a magmatic A-type geochemical signature and were named Volta do Rio Plutonic Suite. Santos et al. (2020) detailed the Volta do Rio Plutonic Suite into two units named Poço Preto and Santa Inês – Volta do Rio.

2.2. Physiographic aspects

The area under study covers partially the counties of Boa Nova, Itagi, Jequié and Dário Meira. It includes the hydrographic basin of the Contas River and it is located in the transition of the biomes Caatinga and Atlantic Forest, with predominance of dry forests as well as dense ombrophilous forest, respectively (INEMA 2019; IBGE 2019). According to the Köppen's climate classification map for Brazil, the region is tropical with dry winter (Aw). The areas with altitudes above 600 meters are humid subtropical, with oceanic influence without dry season, and with hot summer (Cfa) and temperate summer (Cfb) (Alvares et al. 2013).

The geomorphological unit that hosts the bauxite occurrences is called Serras Marginais do Leste da Bahia. It occurs in wide extensions and present extremely dissected slopes, with the presence of embedded valleys, convex slopes

and drainage significantly carved, with features controlled by structural lineaments with NE-SW direction, predominant in the region (IBGE 2021). There are indications of pediplanation processes highlighted in the residual relief of hill tops, originated during the Cretaceous, relative to the Gondwana planation surface (Silva 2009).

3. Materials and methods

The geological mapping was executed through cross-sections with WNW-ESE direction, which is orthogonal to the trend of the main regional structures (ENE-SSW). On the ITJ occurrence, a vertical profile was described and sampled considering the mineralogical and textural characteristics of each identified horizon. The samples of the CDF and VLT occurrences were essentially of bauxite mineralization, but also included other horizons of the lateritic profile. The geographic coordinates from latitude and longitude provided throughout the text are in degrees (°), minutes (') and seconds (") format, with the DATUM GCS_Sirgas2000.

The slope map is a topographic map that shows the variation of elevation per area unit, and it is derived from a digital elevation model (DEM). The source of the data for the DEM confection was the Shuttle Radar Topography Mission (SRTM), which provides the terrain elevation at a spatial resolution of 30 m (Farr et al. 2007). The slope map was calculated from a pixel neighborhood operation using the Google Earth Engine Terrain library.

The stream sediments samples were collected at 59 basins with 10 to 20 km² in length. The sampling stations were defined at the lowest altitude point of each drainage basin (downstream), considering the influence of neighbor streams and avoiding anthropogenic interventions. The preparation and chemical analyses were carried out at the SGS Geosol Laboratory, Vespasiano unit, Brazil. The samples were sieved < 80# (0,175 mm, ranging from thin sand to clay), pulverized to 150# (~ 0.1 mm), digested by hot aqua regia and analyzed by Inductively Coupled Plasma Mass Spectroscopy (ICP-MS) (ICP-MS) and Inductively Coupled Plasma Atomic Emission Spectroscopy (ICP-AES). Using the Statistica 14 and ArcGIS 10.6 softwares, the geochemical results were explored using a range of common statistical techniques including descriptive summary statistics, spearman rank correlation analysis and classified geochemical maps according to Filzmoser et al. (2009) and Liu et al. (2016) recommendations. The factor analysis was performed according to Reimann et al. (2002) and was used to investigate the geochemical trends and associations of the analyzed elements.

Twelve polished thin sections were examined for petrographic characterization of the several horizons of the lateritic profile. The description of the mineral assemblages and its textural characteristics was mainly focused on the determination of the primary mineralogy of the bedrock as well as secondary minerals that occur across the lateritic profile. The modal composition was determined by visual estimation and mineral abbreviations were used according to Whitney and Evans (2010).

The mineral composition of representative samples of the lateritic profile was characterized by X-ray powder diffraction (XRD), using a Bruker AXS model D2 Phaser diffractometer, equipped with a copper anode ($\lambda_{Cu K\alpha} = 1.54184\text{\AA}$), under 30kV-10mA operating conditions at the Laboratory of Mineral

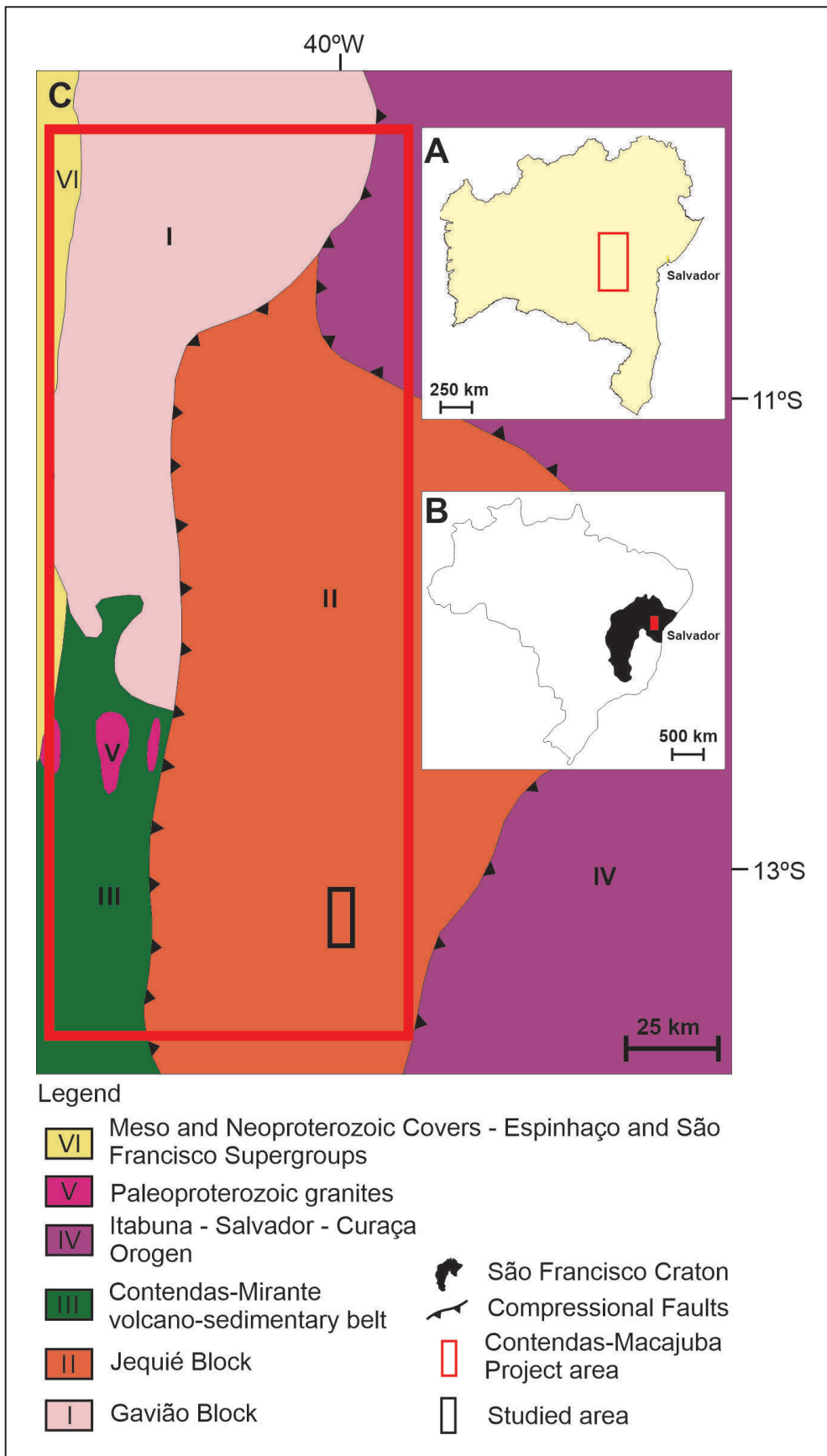


FIGURE 1. São Francisco Craton (SFC) main features. (A) Geographic position of the Contendas-Macajuba Project (CMP, red box highlighted) relative to the Bahia state limits. (B) Geographic position of the SFC relative to Brazil limits. The filled red box highlights the CMP. (C) Main geotectonic units that surrounds the Jequié Block (Modified from Barbosa et al. 2012). The CMP is highlighted by the red box while the studied area by the black box.

Technology - X Ray, member of the Laboratory Complex of Preparation and Analysis of Geoscience Samples (LAPAG), of the Geoscience Institute, Federal University of Bahia, Brazil. The XRD patterns were obtained in the range of $1^\circ - 70^\circ 2\theta$, step of $0.014^\circ 2\theta$ and count of 0.350s/step and were interpreted using the DIFFRAC EVA software.

Twenty rock samples, with mass between one and two kilograms, were analyzed for whole rock geochemical composition at the SGS Geosol Laboratory, Vespasiano unit, Brazil. The massive rock samples were washed to remove superficial dirt, dried to 105°C , crushed to 3 mm in an agate ball mill with 95% passing 150 mesh, homogenized, quartered, and fused with lithium metaborate. The friable rock samples followed the same procedures, with the exception for the washing. The major elements (SiO_2 , Al_2O_3 , Fe_2O_3 , CaO , MgO , TiO_2 , P_2O_5 , Na_2O , K_2O , MnO , ZrO_2) were determined by X-ray fluorescence spectrometry and trace elements (Ba, Cu, Co, Ga, Hf, Mo, Nb, Ni, Rb, Sn, Sr, Ta, Th, Tl, U, V, W, Y, Zn, Zr, Li, Pb, Sc, As, Bi, Ge, Hg, In, P, La, Ce, Pr, Nd, Sm, Eu, Gd, Tb, Dy, Ho, Er, Tm, Yb, Lu), including rare earth elements (REE), by Inductively Coupled Plasma Mass Spectroscopy (ICP-MS). The loss on ignition (LOI) was calculated by weight difference after heating to 1000°C . The results for major elements are presented in weight percent (wt. %); trace and REE, in parts per million (ppm). The degree of weathering or chemical index of alteration (CIA) was calculated using Equation 1 according to Nesbitt and Young (1982), in which the CaO content is controlled by silicate minerals only:

$$\text{CIA} = [\text{Al}_2\text{O}_3 / (\text{Al}_2\text{O}_3 + \text{CaO} + \text{Na}_2\text{O} + \text{K}_2\text{O})] \times 100 \text{ (Equation 1).}$$

The REE values were normalized both to the chondrite from Sun and McDonough (1989) and to the upper continental crust average composition from Rudnick and Gao (2014). The La/Yb ratio was calculated using normalized values according to LaveufandCornu (2009) recommendation. The Ce anomaly, Ce/Ce^* was calculated according to Taylor and McLennan (1985):

$$\text{Ce}/\text{Ce}^* = (2 \times \text{Ce}_N) / (\text{La}_N + \text{Pr}_N)^{0.5} \text{ (Equation 2).}$$

4. Results

4.1. Local geology

In the present study the stratigraphic nomenclature proposed by Santos et al. (2020) was used (Figure 2), in which the lithological substratum is related to the Poço Preto and Santa Inês – Volta do Rio rocks, both re-equilibrated in the granulitic metamorphic facies, of the Jequié Complex from Barbosa (1990). The Poço Preto Unit is composed of meta-granodiorites to metatonalites, with dark gray color (Figure 3A). The primary mineralogy includes plagioclase, potassic feldspar, both usually with mesoperthite exsolution, quartz, amphibole, orthopyroxenes, clinopyroxenes and biotite, while accessory minerals are magnetite, apatite, zircon, chlorite and sericite (Figure 3B). The Santa Inês – Volta do Rio Unit is composed of meta-granites to meta-granodiorites, usually greenish gray to dark gray. The primary mineralogy (Figure 3C) is composed of feldspar, usually with perthite to mesoperthite exsolution, quartz, amphibole, and pyroxene (ortho- and clino-), while accessory minerals include zircon, garnet, apatite, sericite, chlorite, titanite, biotite and magnetite (Figure

3D). The other two units of the Jequié Complex that occur in the region, which were not approached in the present study, are Oriente Novo and Serra do Timorante, both composed of granulitic plutonic rocks.

4.2. Stream sediment

The statistical parameters of each analyzed element were calculated (Table 1) and in the following sections the results that are relevant to further geological discussions are described (Figure 4).

The univariate analysis of statistical summary shows some elements with results below Detection Limit (DL) and/or censored data, which will not be assessed in bivariate and multivariate treatment stages. In addition, it was possible to observe an asymmetric behavior of the distribution showing the need for logarithmic transformation in order to compensate for the asymmetrical distribution.

The Al and Fe present the highest contents in the catchments of the central portion of the studied region, where the parent rocks of bauxite mineralization occur, while Ca, K and Mg are present with low contents in the samples collected in this region and high concentrations associated with Povoado Oriente Novo and Povoado Nova Esperança rocks, both from the Jequié Complex (Figure 5).

The highest contents of Zr, Hf, Nb, high field strength elements, in addition to Th, occur in catchments adjacent to the laterite profiles studied, mainly in the northern portion of the region, but also occur in the southern portion. Other elements, such as Rb, present lower contents in these regions (Figure 6).

The REE content, in addition to Y and Sc, reaches up to 700 ppm in the studied samples, with Ce being the most abundant element with concentrations of up to 399 ppm. This set of elements has the highest levels in the northern portion of the study area, mainly in the region of the Itaji and Casa da Farinha profiles, with Ce and La also high in the area of the Valentim profile (Figure 7).

The relationship between the variables was assessed by correlation analysis using the Spearman rank of log-transformed data and scatter plots. The Figure 8 shows scatter plots of some representative elements, which exhibited good linear relationships after log transformation.

There is a high positive correlation between Ce, Th and U, in addition to Nb and Ti. When HREE were analyzed, the positive correlation was better defined with Fe. Fe also shows good correlation with Al and these two elements are correlated to Sc, V and P.

On the other hand, there is a negative correlation between the elements mentioned above, mainly Nb, Sn, Ti with Ca, K, Mg, in addition to Rb and Cs (Figure 8), showing an opposite tendency of enrichment of elements with high ionic potential and leaching of those with low potential and greater mobility in the surface environment, during the weathering processes.

The factor analysis was applied to the geochemical dataset and twenty-nine elements were evaluated and four factors were obtained. These four factors correspond to 81.55% of the total system variance. Each factor consists of the elements with the highest correlation, or highest factor loading, which are expressed in Figure 9.

The geochemical associations of elements in the stream sediments, defined by factor analysis were used as reference

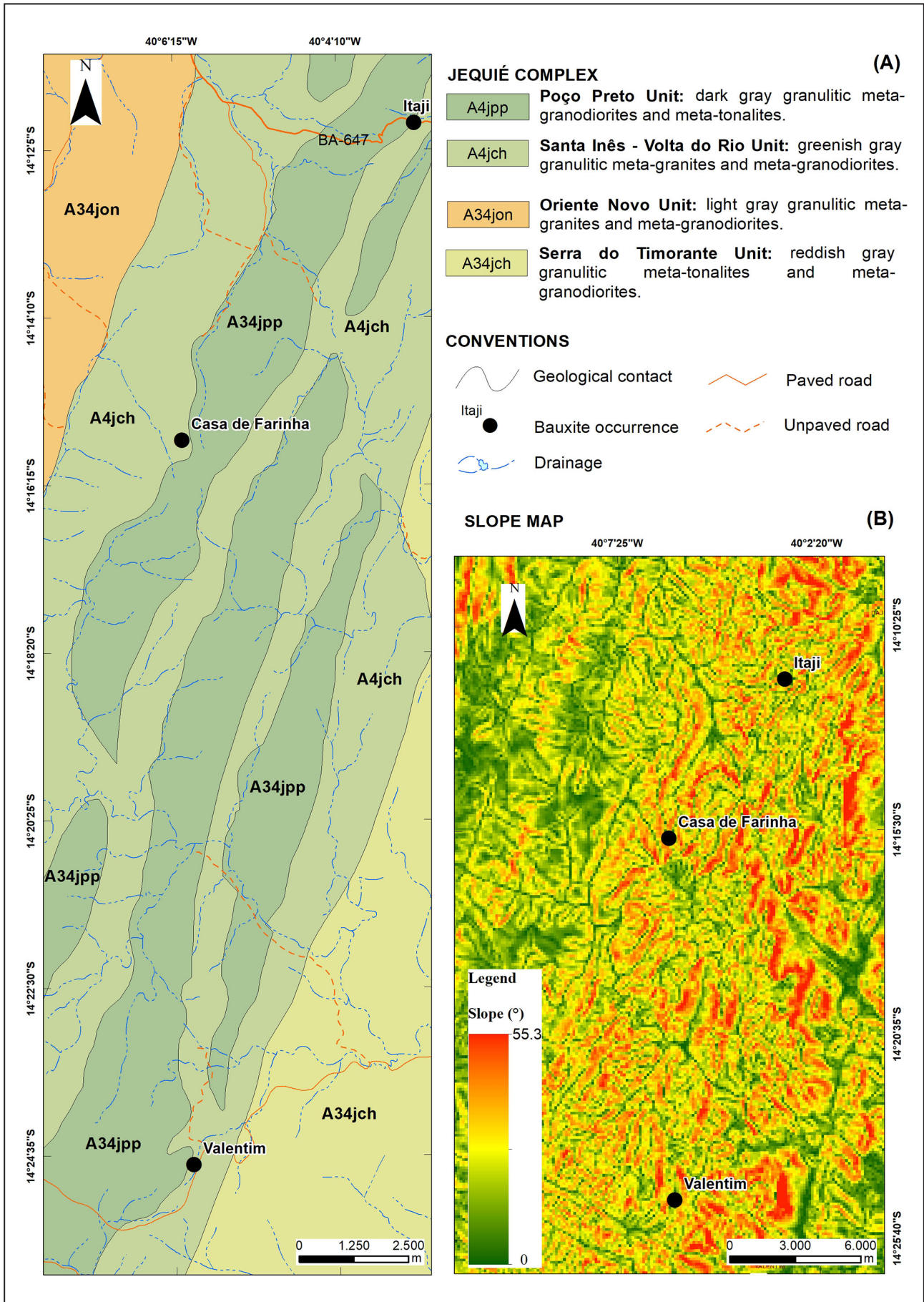


FIGURE 2. (A) Simplified geological map of the region of bauxite occurrences. (B) Slope Map of the region, based on the results from Farr et al. (2007).

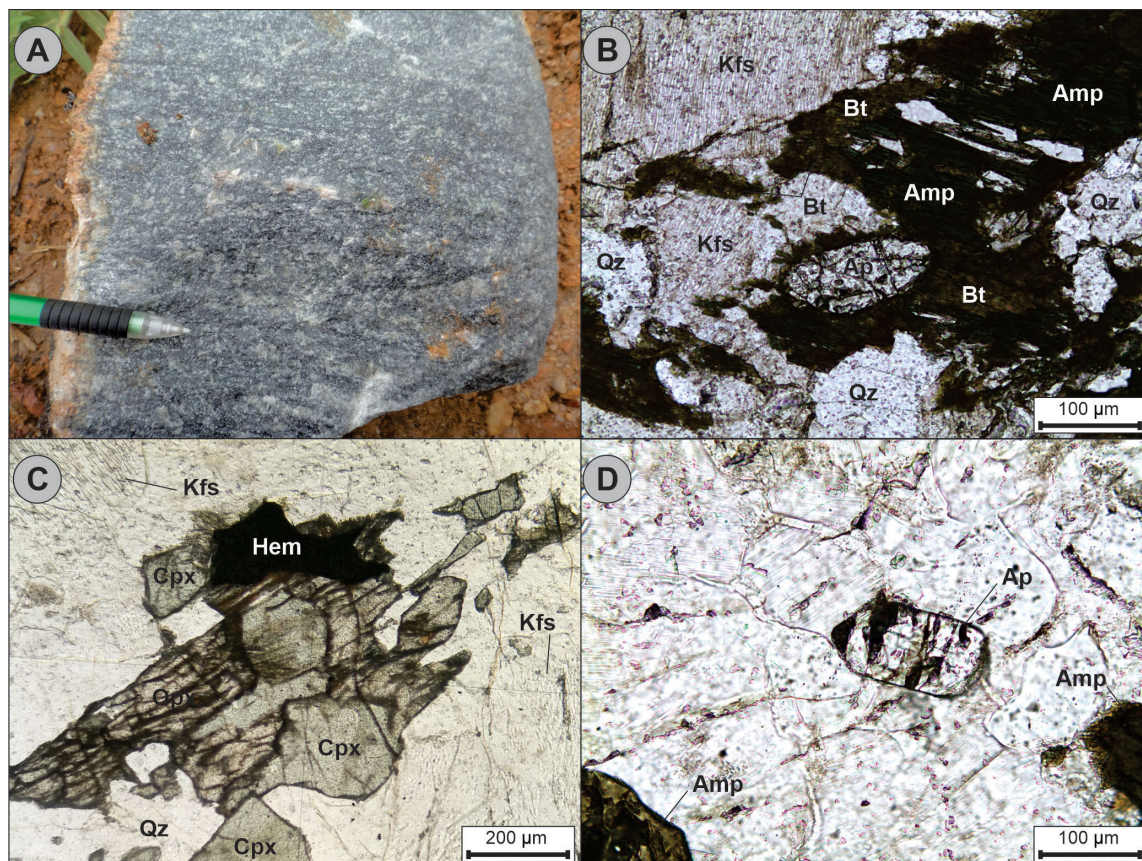


FIGURE 3. General features from the Poço Preto and Santa Inês – Volta do Rio Units. (A) Macroscopic aspect of the metagranodiorites to metatonalites. (B) The Poço Preto predominant mineral association is represented by potassic feldspar (Kfs), amphibole (Amp), biotite (Bt), quartz (Qz), and the apatite (Ap) is representing part of the accessory mineralogy. (C) Santa Inês – Volta do Rio primary mineralogy represented by the potassic feldspar (Kfs), orthopyroxene (Opx), clinopyroxene (Cpx), quartz (Qz) and the hematite (Hem) crystal is representing part of the accessory mineralogy. (D) Detail of the apatite (Ap) crystal which occurs isolated from the amphibole crystals (Amp).

TABLE 1. Statistical summary for geochemical dataset. UCC: upper continental crust average composition from Rudnick and Gao (2014).

Elements	Detection Limit	% Censored data	% of Valid N	Minimum	25%	Median	Mean	75%	Maximum	Standard Deviation	UCC
Al (%)	0.01	0.00	100.00	0.19	0.70	1.03	1.02	1.56	4.78	2.04	8.15
As (ppm)	1.00	67.80	32.20	0.50	0.50	0.50	0.73	1.00	3.00	1.81	4.80
Ba (ppm)	5.00	0.00	100.00	9.00	21.00	30.00	34.05	55.00	339.00	2.07	624.00
Be (ppm)	0.10	15.25	84.75	0.05	0.10	0.20	0.20	0.40	1.20	2.32	2.10
Bi (ppm)	0.02	20.34	79.66	0.01	0.02	0.03	0.03	0.04	0.20	2.06	0.16
Ca (%)	0.01	3.39	96.61	0.01	0.02	0.03	0.04	0.08	0.87	3.10	2.56
Cd (ppm)	0.01	0.00	100.00	0.01	0.02	0.03	0.04	0.06	0.58	2.19	0.09
Ce (ppm)	0.05	0.00	100.00	18.29	41.06	61.91	70.31	127.70	399.72	2.12	63.00
Co (ppm)	0.10	0.00	100.00	0.70	1.90	3.00	3.17	5.00	27.40	2.30	17.30
Cr (ppm)	1.00	0.00	100.00	5.00	12.00	21.00	20.76	33.00	125.00	1.98	92.00
Cs (ppm)	0.05	30.51	69.49	0.03	0.03	0.08	0.08	0.14	1.07	2.52	4.90
Cu (ppm)	0.50	0.00	100.00	0.70	3.20	4.90	5.34	9.20	44.60	2.14	28.00
Fe (%)	0.01	0.00	100.00	0.48	1.38	2.46	2.18	3.47	9.64	1.91	3.91

TABLE 1. Statistical summary for geochemical dataset. UCC: upper continental crust average composition from Rudnick and Gao (2014). (continued).

Elements	Detection Limit	% Censored data	% of Valid N	Minimum	25%	Median	Mean	75%	Maximum	Standard Deviation	UCC
Ga (ppm)	0.10	0.00	100.00	0.70	3.50	5.80	5.68	8.90	25.10	2.09	17.50
Hf (ppm)	0.05	23.73	76.27	0.03	0.03	0.10	0.13	0.33	2.18	3.84	5.30
Hg (ppm)	0.01	0.00	100.00	0.01	0.05	0.07	0.06	0.10	0.19	1.78	0.05
In (ppm)	0.02	45.76	54.24	0.01	0.01	0.02	0.02	0.04	0.10	2.15	0.06
K (%)	0.01	25.42	74.58	0.01	0.01	0.02	0.02	0.03	0.11	2.51	2.32
La (ppm)	0.10	0.00	100.00	9.00	18.50	27.10	33.85	71.30	255.00	2.22	31.00
Li (ppm)	1.00	52.54	47.46	0.50	0.50	0.50	0.95	2.00	5.00	2.21	20.00
Lu (ppm)	0.01	3.39	96.61	0.01	0.03	0.06	0.06	0.09	0.30	2.46	0.31
Mg (%)	0.01	28.81	71.19	0.01	0.01	0.02	0.02	0.05	0.40	3.24	1.49
Mn (ppm)	5.00	1.69	98.31	68.00	145.00	231.00	287.90	428.00	10000.00	2.57	775.00
Mo (ppm)	0.05	0.00	100.00	0.24	0.52	0.88	0.94	1.83	3.57	2.08	1.10
Na (%)	0.01	66.10	33.90	0.01	0.01	0.01	0.01	0.01	0.08	2.11	2.42
Nb (ppm)	0.05	0.00	100.00	0.35	1.14	3.83	2.80	5.95	14.42	2.80	12.00
Ni (ppm)	0.50	0.00	100.00	0.70	2.80	4.30	4.93	8.90	135.10	2.63	47.00
P (ppm)	50.00	0.00	100.00	61.00	134.00	207.00	201.32	293.00	738.00	1.80	655.00
Pb (ppm)	0.20	0.00	100.00	5.70	8.60	11.10	11.30	13.90	55.50	1.48	17.00
Rb (ppm)	0.20	0.00	100.00	0.30	0.80	2.00	1.97	4.20	16.40	2.76	0.82
S (%)	0.01	28.81	71.19	0.01	0.01	0.02	0.02	0.04	0.29	2.99	0.06
Sb (ppm)	0.05	77.97	22.03	0.03	0.03	0.03	0.03	0.03	0.36	2.06	0.40
Sc (ppm)	0.10	0.00	100.00	0.60	2.10	3.20	3.21	5.20	14.00	1.99	14.00
Sn (ppm)	0.30	0.00	100.00	0.40	0.80	1.20	1.16	1.70	3.30	1.62	2.10
Sr (ppm)	0.50	0.00	100.00	1.00	2.50	4.20	5.04	9.50	42.40	2.28	320.00
Tb (ppm)	0.02	0.00	100.00	0.08	0.19	0.30	0.35	0.73	2.24	2.29	0.70
Th (ppm)	0.10	0.00	100.00	1.90	10.40	15.80	18.65	34.70	149.80	2.48	10.50
Ti (%)	0.01	1.69	98.31	0.01	0.05	0.13	0.11	0.26	0.66	3.08	0.38
Tl (ppm)	0.02	23.73	76.27	0.01	0.02	0.04	0.04	0.08	0.47	2.84	0.90
U (ppm)	0.05	0.00	100.00	0.17	0.65	1.06	1.22	1.99	8.21	2.35	2.70
V (ppm)	1.00	0.00	100.00	6.00	16.00	25.00	24.47	38.00	99.00	1.80	97.00
W (ppm)	0.10	47.46	52.54	0.05	0.05	0.10	0.09	0.20	0.70	2.07	1.90
Y (ppm)	0.05	0.00	100.00	1.23	3.63	6.20	6.42	12.85	40.90	2.31	21.00
Yb (ppm)	0.10	6.78	93.22	0.05	0.20	0.50	0.43	0.80	2.60	2.56	2.00
Zn (ppm)	1.00	0.00	100.00	6.00	18.00	23.00	24.18	38.00	61.00	1.65	67.00
Zr (ppm)	0.50	8.47	91.53	0.25	2.20	5.50	4.83	12.80	69.90	4.31	193.00

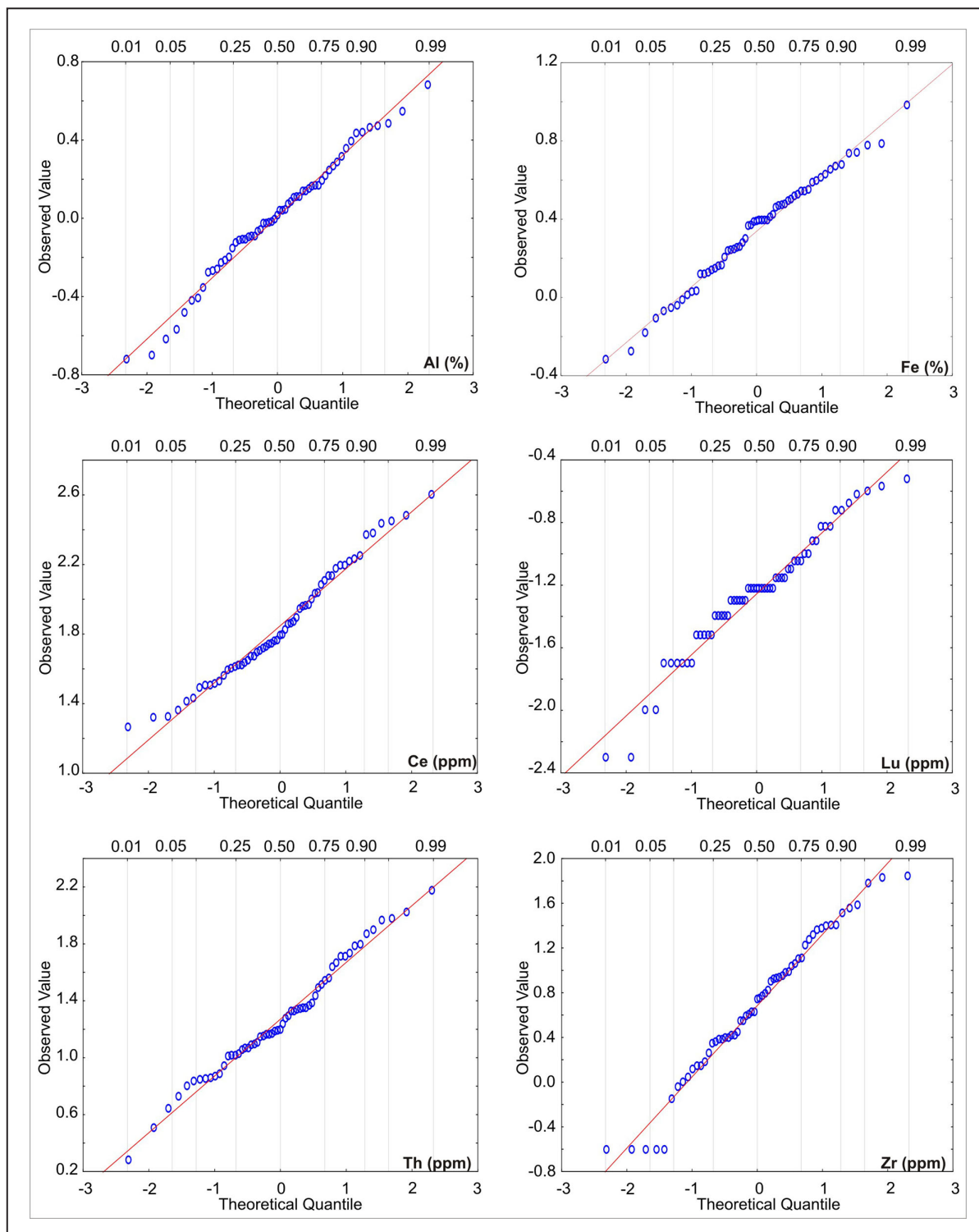


FIGURE 4. QQ plots for representative analyzed elements.

for the construction of multi-element association geochemical maps (Figure 10).

The main factor corresponded to 47.9% of the variance and was dominated by positive loadings for Ce, La and Tb in addition to Th, U, Nb, Ti, Hf e Zr, in other words REE, actinides and some HFSE. As illustrated in Figure 10, the catchments dominated by the highest scores of this association show high consistency with areas of occurrence of the lateritic profiles studied, in addition to a portion further north. The negative loadings for this factor correlate with the outcrop areas of

Oriente Novo rocks (Jequié Complex) and must reflect the primary mineralogy of the rocks, mainly feldspars and micas. In this factor, elements of low ionic potential and high mobility in the surface environment are aggregated, such as K, Ca, Mg, Rb and Cs (Goldschmidt 1937, Nesbitt et al. 1980, Yuste et al. 2017).

The second factor explains 21.4% of the variance and associates, with positive loadings, Al-Ga-Fe-Sc-V-Mo, suggesting close correlation to the weathering processes of bauxitic profile formation. Highest positive scores for

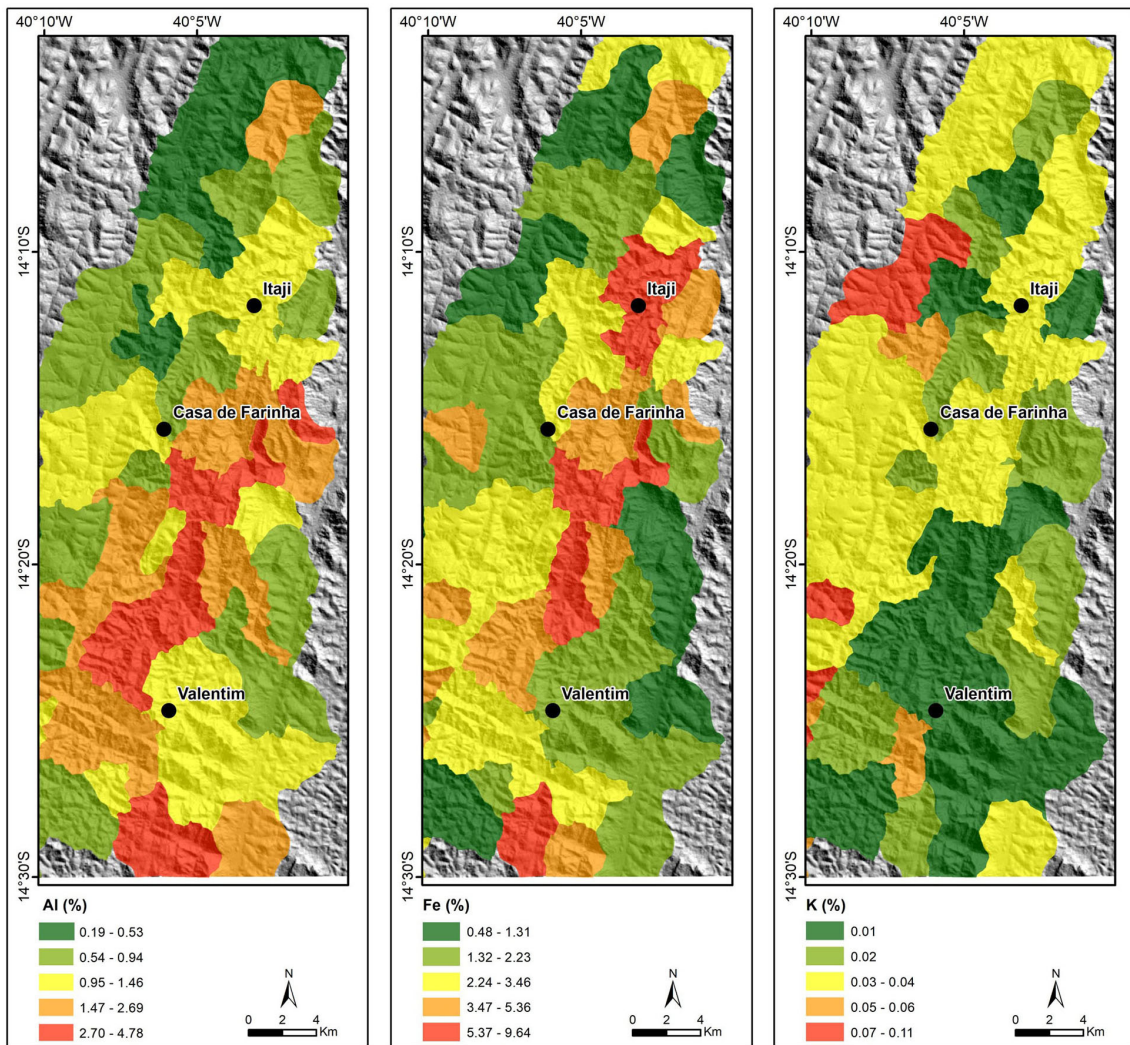


FIGURE 5. Geochemical maps for representative major elements.

this factor outline the central portion of the studied area, mainly to the west and south of the Valentim and Itaji profiles (Figure 10).

The analysis also showed the grouping of Lu, Yb and Y with positive loadings in the third factor. This factor explained 7.05% of the variance and its highest scores plotted in catchments present a good correlation with the occurrence of the studied bauxitic profiles and with the first factor, mainly in the northern portion (Figure 10).

Finally, the fourth factor, which accounts for 5.4% of the variance, associated elements of distinct characteristics in relation to ionic potential, with significant negative loadings, elements of high ionic charge Hf, Zr, Nb and Ti. On the other hand, there are elements of large ionic radius such as P-Ba-Sr-Mg-Ca and they have their highest positive scores in the central portion of the area of the Casa de Farinha profile (Figure 10).

4.3. Geology and mineralogy of the lateritic profile and of bauxite occurrences

The ITJ profile is located on the southern side of the BA-647 road (Figure 11), at the geographic coordinates 14°11'45",

40°03'10", and it is situated at the bottom of a hill slope. The Slope Map of the area indicate angles between 12° and 18° (Figure 2B).

Five horizons were identified (Figure 12). Horizon (i) is the bedrock, composed of light gray meta-granite, with feldspar, quartz and mafic minerals (Figure 13A) which are arranged in a phaneritic texture. The petrography reveals potassic feldspar (55%), quartz (22%) and kaolinite (15%) as the main constituents of the rock (Figure 13B), with accessory mineralogy represented by biotite (2%), amphibole (2%), zircon (1%), apatite (1%), titanite (trace) and an association of magnetite and hematite (2%). The feldspar is perthitic and usually altered to kaolinite, while the quartz is anhedral and occurs between the feldspar crystals. The biotite, amphibole and apatite often occur as pseudomorphic (or relict) crystals immersed in kaolinite (Figure 13C-D), while zircon (Figure 13E), titanite, magnetite and hematite crystals (Figure 13F) occur disseminated in the rock.

The horizon (ii) is composed of a compact sandy silt matrix with pink to pale yellow color, and with rock fragments (Figure 14A) which comprises partially weathered minerals from the substratum rock relicts (Figure 14B). The petrographic

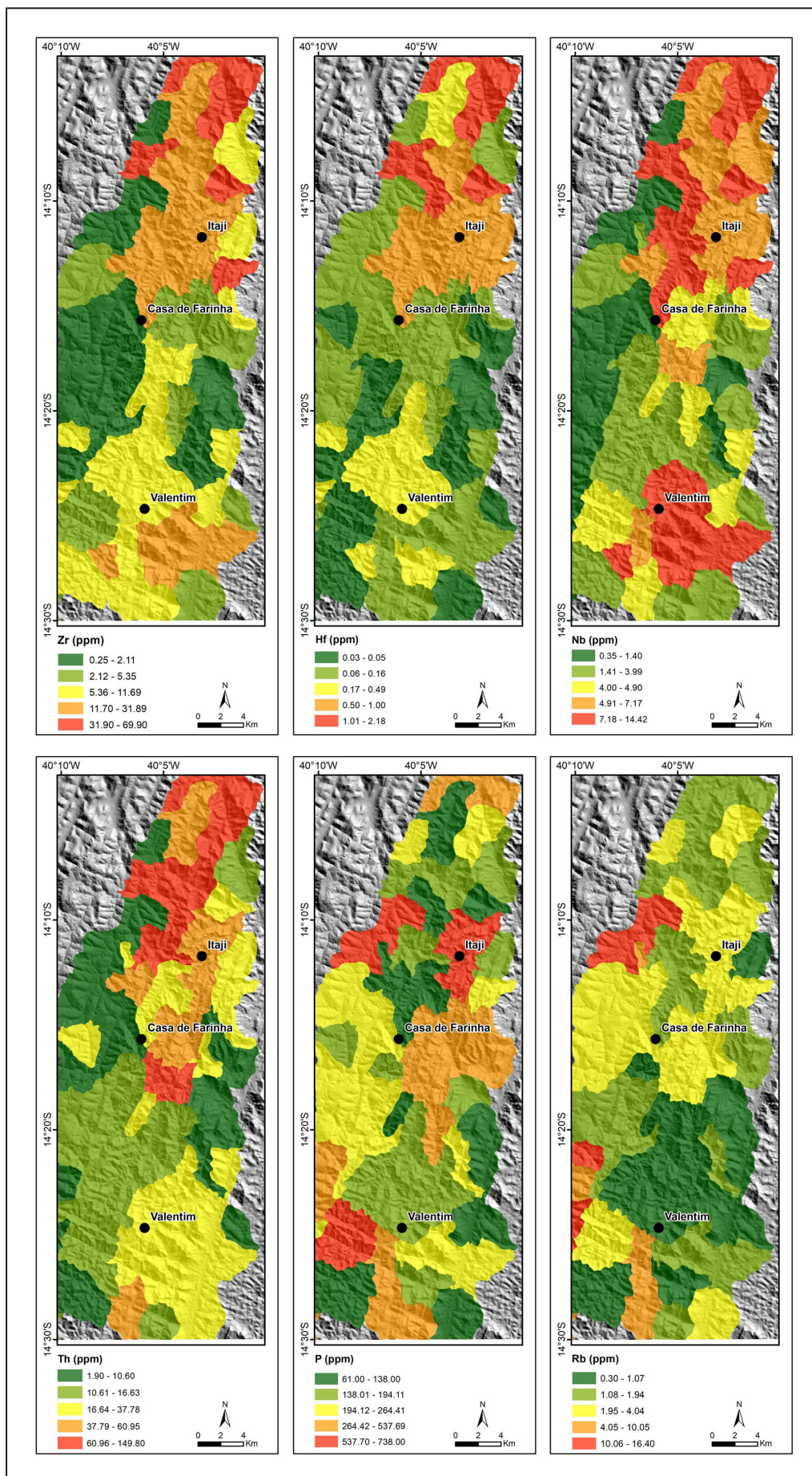


FIGURE 6. Geochemical maps for representative minor and trace elements.

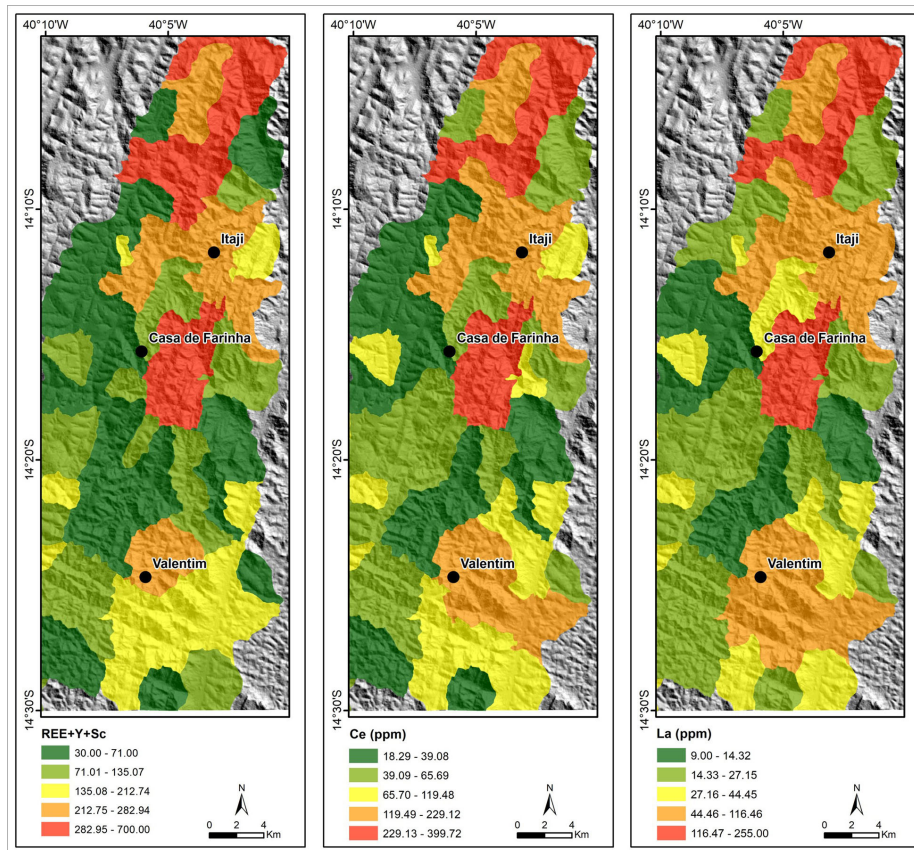


FIGURE 7. Geochemical map for the contents of REE+Y+Sc and geochemical maps for Ce and La.

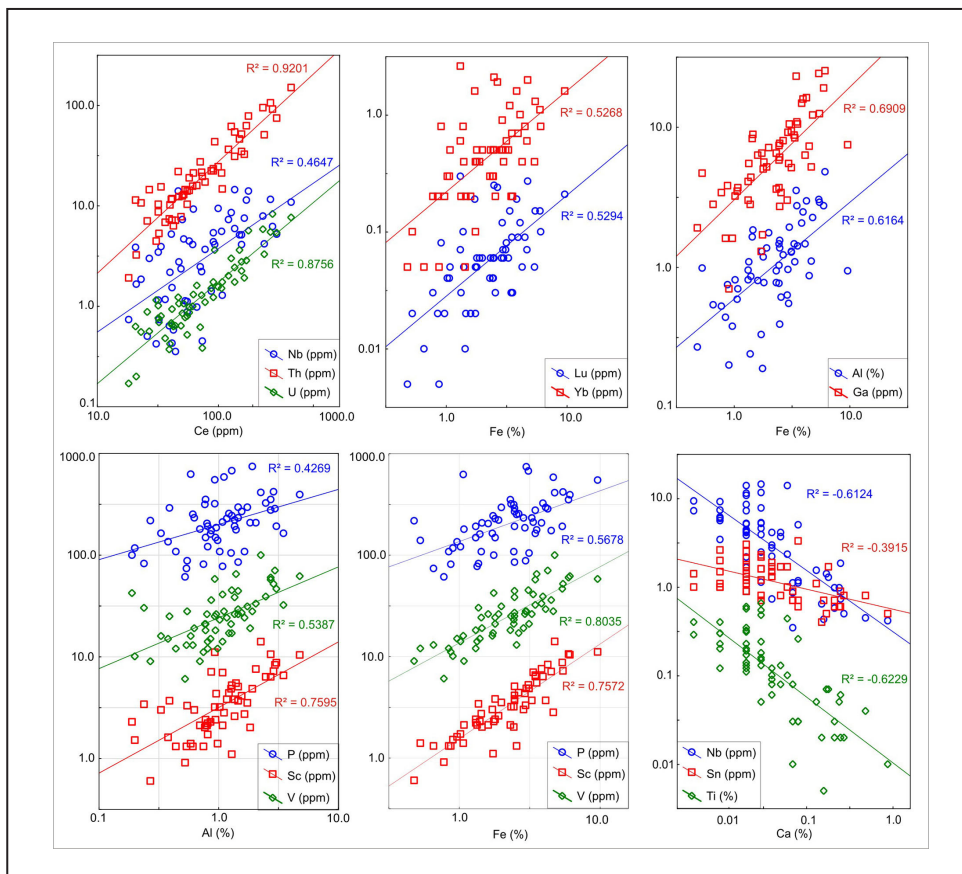


FIGURE 8. Scatter plots of some representative elements.

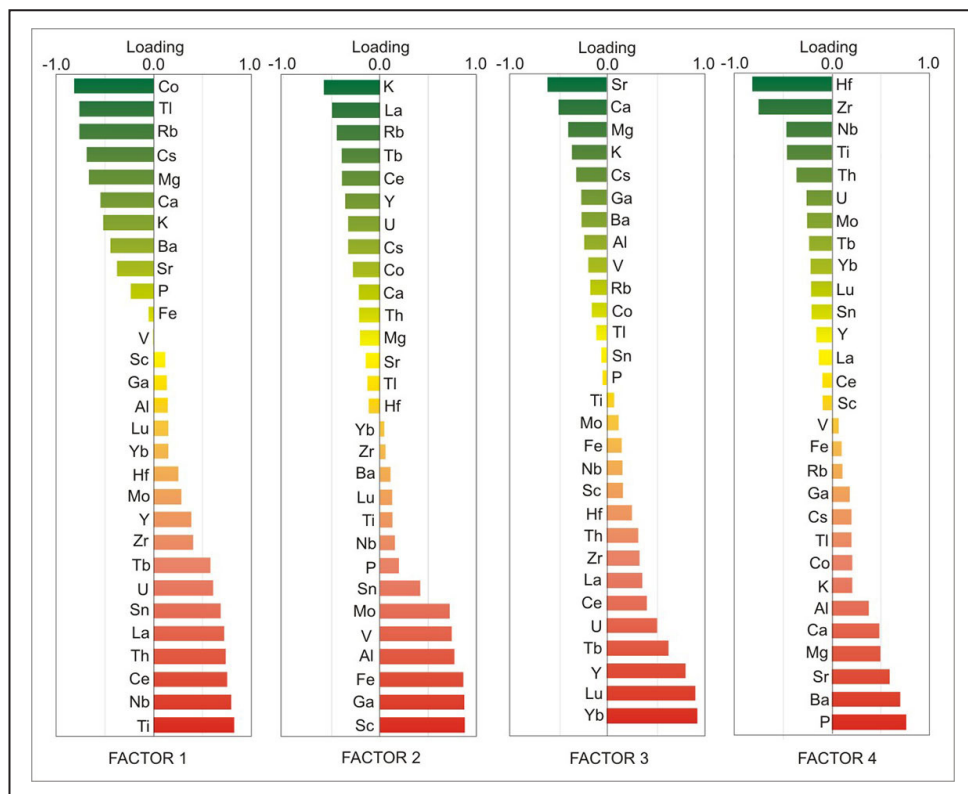


FIGURE 9. The factor loadings of factor analysis carried out with 29 elements. Only elements with factor loadings higher than 0.50, were used.

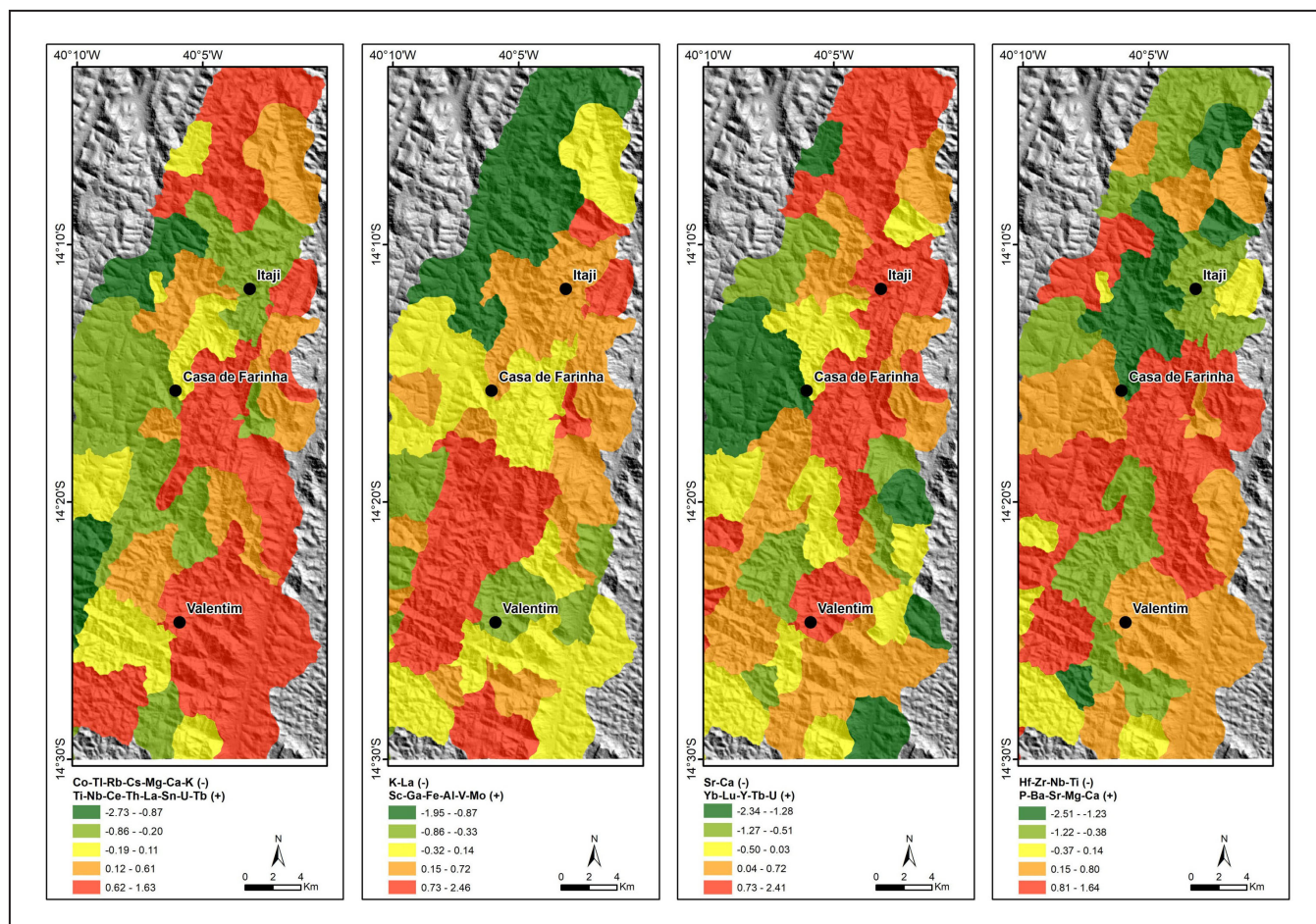


FIGURE 10. The factor loadings of factor analysis carried out with 29 elements. Only elements with factor loadings higher than 0.50, were used.

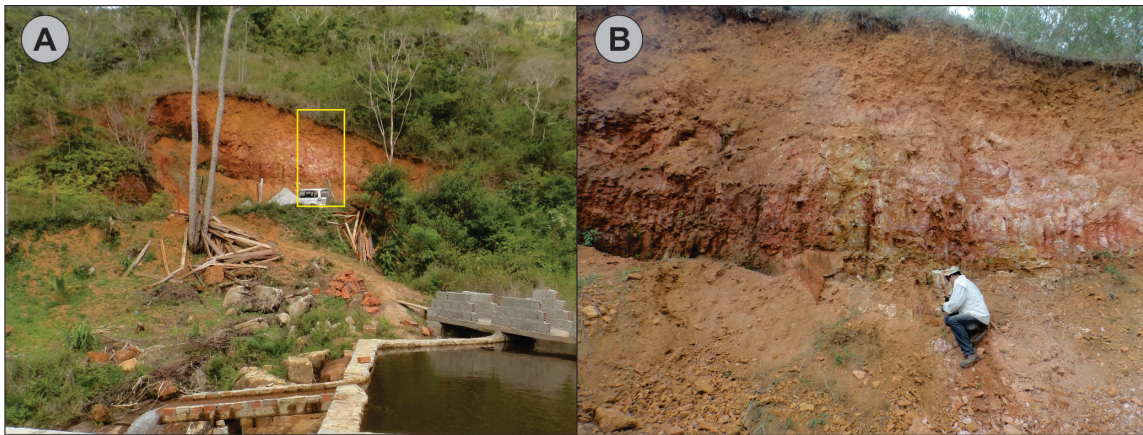


FIGURE 11. (A) General overview from the area. Note that it is located at the bottom of a hill slope. The location of the profile is highlighted by the yellow box. (B) Closer view from the studied vertical profile.

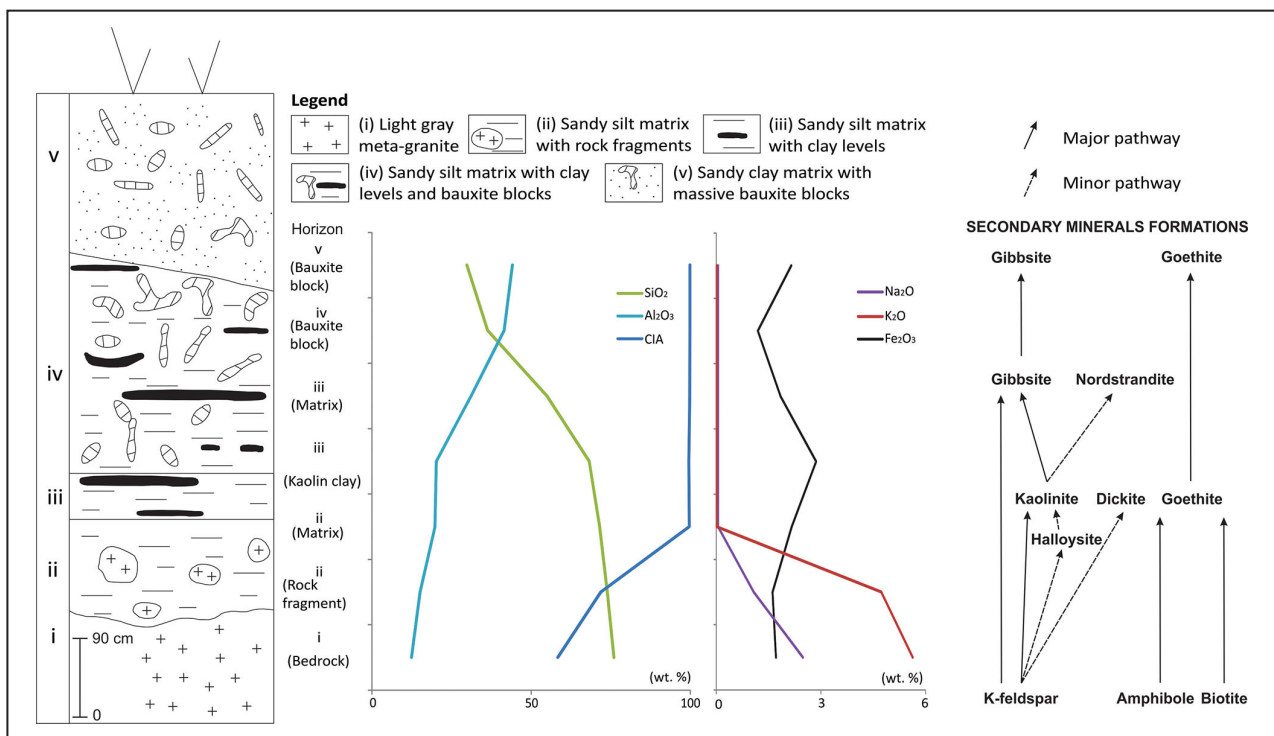


FIGURE 12. Schematic representation of the vertical profile at the Itaji occurrence. The major element results are placed in the vertical position to compare with the geology and are presented in weight percent (wt. %). CIA (chemical index of alteration), calculated according to Nesbitt and Young (1982). The major and minor pathways of the secondary mineral formations are represented by the continuous and dashed lines respectively. The major pathways represent the most predominant mineral transformations, while the minor ones highlight the local observations.

characteristics of the rock relicts are quite similar to horizon (i), except for the absence of apatite.

On horizon (iii), the sandy silt matrix is friable, but the structure of the bedrock is present. It is pink to pale yellow (Figure 14C), and with white to gray levels of kaolin-like clay (Figure 14D). The XRD results indicate quartz and kaolinite as the constituents of the friable matrix (Figure 15A), while the kaolin-like levels are composed of quartz, kaolinite and metahalloysite (Figure 15B).

The horizon (iv) is composed of a pink to pale yellow, friable sandy silt matrix. Supported by this matrix, there are several massive fragments of white to gray bauxite. The fragments are of the size of a block, show irregular shape and are rounded to subrounded (Figure 16A-B), displaying a conglomerate-

like texture. The texture of the bedrock is no longer present in this horizon. The XRD results indicate quartz and kaolinite as the constituents of the friable matrix. The massive bauxite petrography (Figure 16C) showed a microcrystalline matrix, with parallel lamination, composed of gibbsite (80%), kaolinite (10%), with crystals of quartz (5%), goethite and hematite association (5%), titanite and zircon (trace). Also, in the matrix there are kaolin-like pseudomorphs, with pale blue color, that resembles feldspars crystals. The quartz crystals are fine to coarse, intensively fractured. The fractures are filled with gibbsite from the matrix (Figure 16D). The zircon grains occur as prismatic crystals with high birefringence, with the major axis parallel to the lamination of the matrix. The titanite crystals also

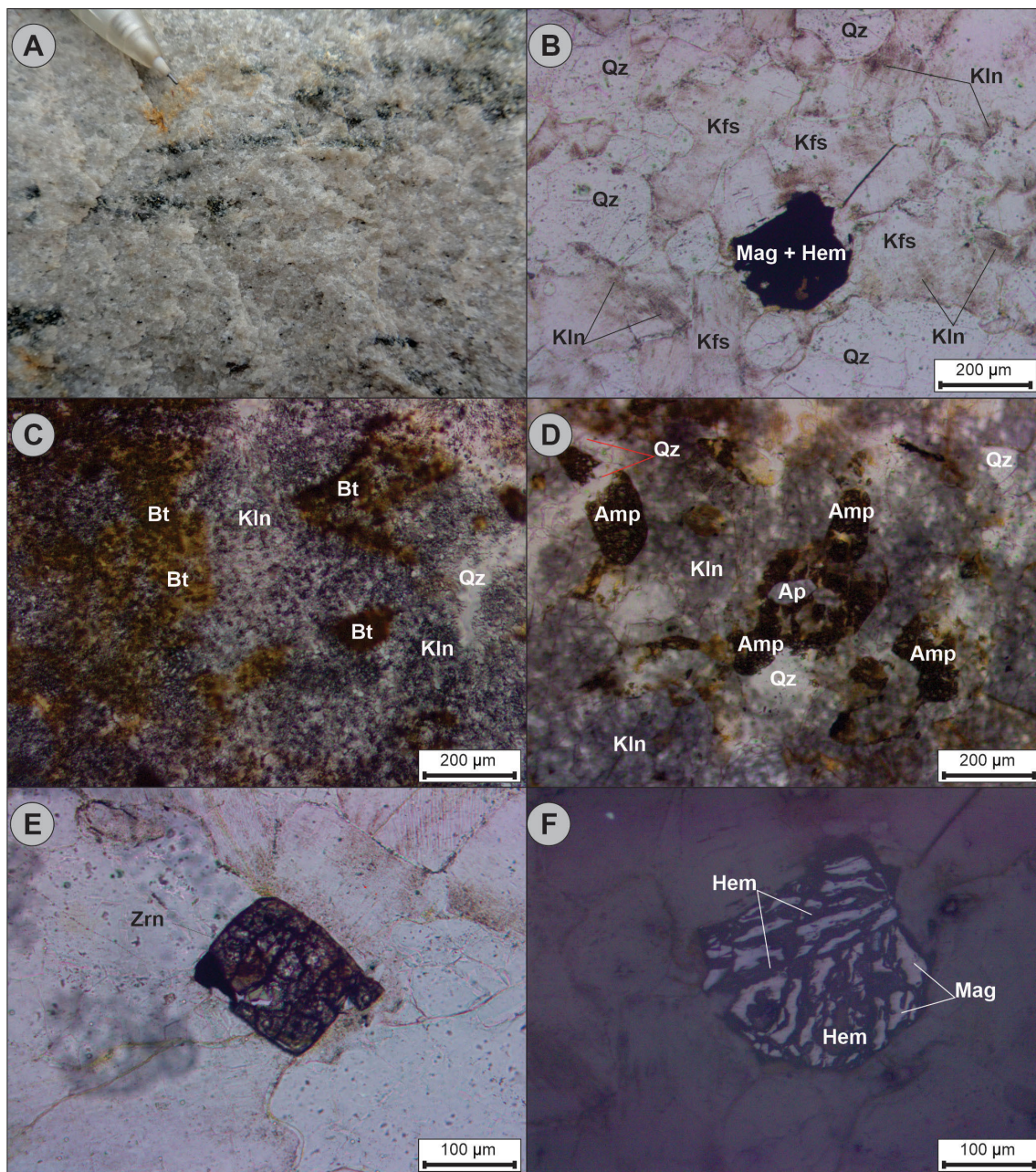


FIGURE 13. Main petrographic features of the horizon (i). (A) Macroscopic detail of the light gray granite. (B) The predominant mineral association represented by the potassic feldspar (Kfs), quartz (Qz) and kaolinite (Kln). (C) Biotite (Bt) relicts immersed in the kaolinite. (D) Amphibole (Amp) and apatite (Ap) crystals immersed in the kaolinite. (E) Isolated zircon (Zrn) crystal. (F) Association of magnetite (Mag) and hematite (Hem).

occur parallel to the lamination of the matrix, and the hematite is altered to goethite. The XRD result from the massive bauxite indicates gibbsite and quartz as the constituents (Figure 15C) while the matrix consists mainly of quartz, kaolinite and gibbsite.

The horizon (v) is composed of a duricrust-like sandy matrix, brown to reddish (Figure 16E), with subrounded to angular blocks of massive bauxite, with grey to reddish color (Figure 16F), and with irregular shape. The petrography of the massive bauxite is similar to those of horizon (iv), but the gibbsite content is lower (75%), quartz (15%) and goethite (10%) are relatively more present, while zircon (trace) and titanite (trace) showed no difference in their proportion. The XRD results from both duricrust and massive bauxite indicate gibbsite and quartz as the main constituents of this horizon.

The CDF bauxite occurrence is at the top of the hill (Figure 17A), at the geographic coordinates $14^{\circ}15'40''$, $40^{\circ}06'08''$, and there is an unpaved road that passes through it (Figure 17B). The Slope Map of the area indicate angles between 6° and 8° (Figure 2B). Two horizons were identified and are described following the same nomenclature used on the ITJ profile considering the macroscopic similarities between them. Horizon (iii) is composed of a friable sandy silt matrix, pink to pale yellow and white with levels of kaolin-like clay. The XRD results indicate quartz and kaolinite as the constituents of the friable matrix, while quartz, kaolinite and halloysite are the main ones for the levels of kaolin-like clay. Horizon (iv) is composed of gray to reddish blocks of massive bauxite (Figure 17C-D), and XRD results indicate



FIGURE 14. Main textural features of the horizons (ii) and (iii). (A) Bedrock relict. (B) Detail on the weathered rock fragment. (C) Variation in the color of the horizon (iii). (D) Interlayers of kaolin-like clays.

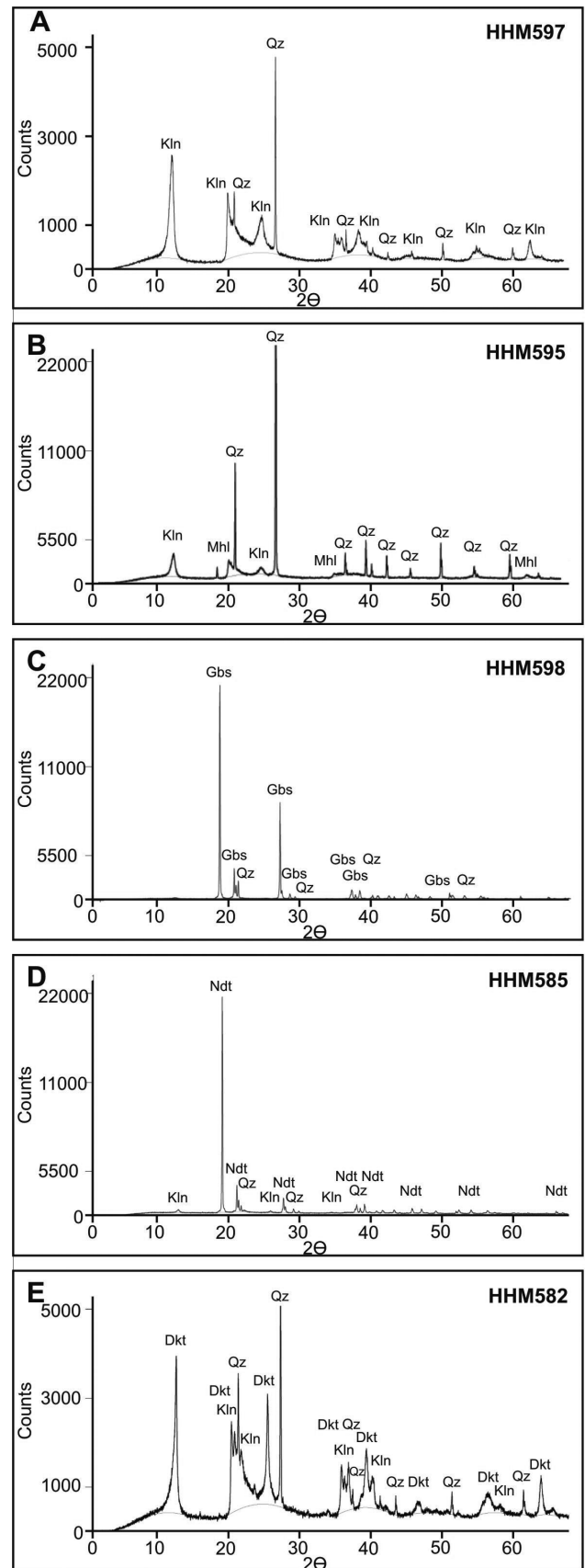


FIGURE 15. Selected X-ray diffractograms of the main horizons identified at the Itaji vertical profile (A-C), and at Casa de Farinha (D) and Valentim (E) occurrences. Abbreviations: Klin (kaolinite), Qz (quartz), Mhl (metahalloysite), Gbs (gibbsite), Ndt (nordstrandite), Dkt (dickite). The labels of the samples are placed on the upper right corner of each diffractogram.

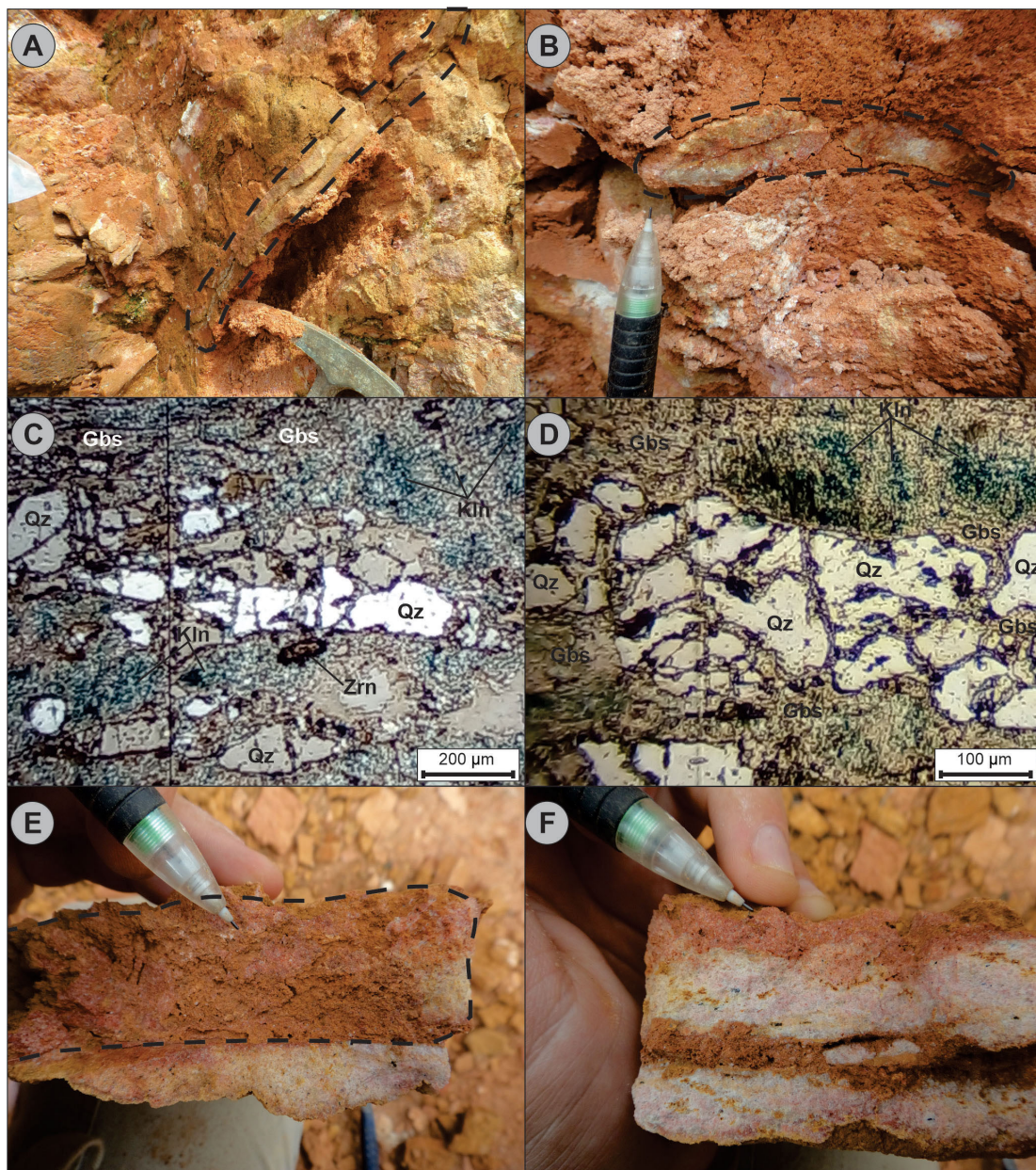


FIGURE 16. Main features of horizons (iv) and (v). (A-B) General view from the massive blocks of bauxite in the horizon (iv) (dashed line highlighted). (C) Intensively fractured quartz (Qz) crystals immersed in matrix composed of gibbsite (Gbs) and kaolinite (Kln). Note the zircon (Zrn) in the central lower portion of the photomicrograph with the major axis parallel to the quartz crystals. (D) Closer view of the fractures of the quartz (Qz) filled by the gibbsite from the matrix. The kaolinite (Kln) accumulation in the upper portion of the photomicrograph resembles a relict feldspar crystal. (E) Closer view from the duricrust-like matrix of the horizon (v) (dashed line highlighted). (F) Blocks of massive bauxite with reddish color of the horizon (v).

nordstrandite, kaolinite and quartz (Figure 15D) as main constituents.

The VLT occurrence is located at the geographic coordinates 14°24'31", 40°05'84'. The outcrop is on the eastern side of the unpaved road that passes through it. The Slope Map of the area indicates angles between 8° and 10° (Figure 2B). Two horizons were identified, also with very similar characteristics of horizons (iii) and (iv) from the ITJ profile (Figure 17E-F), thus the same nomenclature is followed and, in this case, we only mention the difference between them, which is the presence of dickite in the XRD results (Figure 15E) on the levels of kaolin-like clay on horizon (iii).

4.4. Whole rock geochemistry

The complete results of whole rock geochemistry of the ITJ, CDF and VLT samples are presented in Table 2, and in the following sections only the results that are relevant to further geological discussions are described.

4.4.1. High Field Strength Elements

In terms of the ITJ vertical profile, the Zr (Figure 18A), Hf (Figure 18B) and Ta (Figure 18C) presented an increase, mainly related to horizons (ii) and (iii), while Nb (Figure 18B) and W (Figure 18C) showed a sharp increment related to



FIGURE 17. Main features of the Casa de Farinha (CDF) and Valentim (VLT) occurrences. General view from the area of the CDF occurrence (A), and the bauxite outcrop (B) in the middle of the road. Closer view of the in situ bauxite outcrop (C) and of some collected samples (D) at CDF. Detail of horizon (iii) with levels of kaolin-like clay (E), and of the gray massive block of bauxite (F) at VLT.

the friable matrix of horizon (ii). The Th presented a non-continuous content increasing upwards the profile (Figure 18D). The contents of High Field Strength Elements (HFSE) previously described surpassed the values of the rock substratum, except for W content on horizon (v).

The contents of the HFSE on horizons (iii) and (iv) from the CDF and VLT occurrences, are higher than the UCC composition, except for Ta and Th. In the case of Th, despite that half of the results are lower than the UCC, three samples presented values above it.

4.4.2. Rare earth elements

In terms of the ITJ vertical profile, the light rare earth elements (LREE) showed a peak in the horizon (iii), quite similar for the Ce content. The heavy rare earth elements (HREE) are enriched in

the bedrock and showed a continuous decrease from the bottom to the top of the profile (Figure 18). On the other hand, the friable matrix of horizon (iii) and the bauxite block of horizon (v) presented a sharp increment in Ce content. Another characteristic is the fractionation between LREE and HREE. All the values of the La/Yb ratio normalized to the UCC were above 1.

Considering the comparison between the results from the CDF and VLT samples with the UCC, most of the samples presented the REE content close to the values of UCC, or above it. The exception is represented by samples from the CDF occurrence that showed REE contents very close, or below the values of UCC. In terms of Ce content, all the samples presented values above the UCC composition, except for samples from CDF.

Considering the normalized values both to chondrite and to the UCC, most samples showed Ce positive anomaly, except for the results of samples from the ITJ profile and CDF.

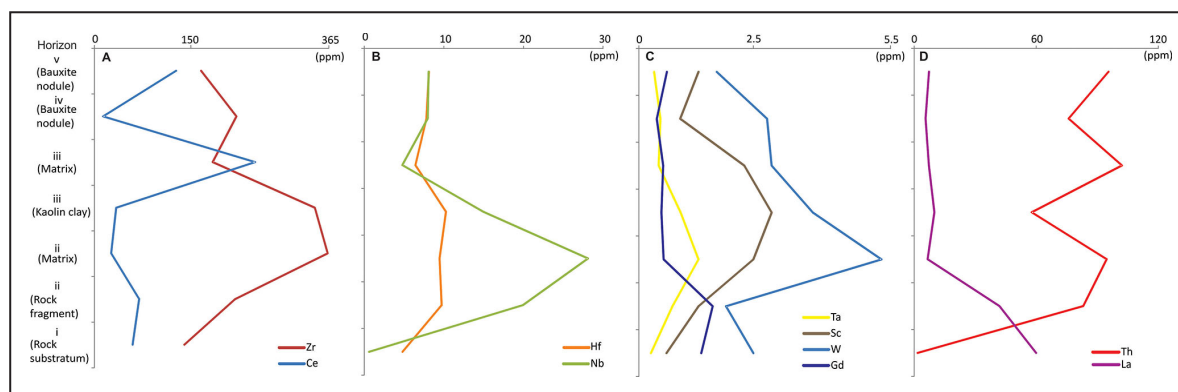


FIGURE 18. Main trace elements, and rare earth elements of the ITJ vertical profile. The horizons are placed vertically for comparison with the geological profile of Figure 12. The results are presented in parts per million (ppm).

5. Discussion

5.1. Stream sediments

The geochemical maps for major elements indicate the enrichment of Al and Fe in the region where bauxite occurs. The low K content associated with negative correlation observed between Ca, K, Mg with these elements and others confirms the tendency of leaching of alkaline cations from the weathering profile. According to Nesbitt et al. (1980) and Mordberg (1996), most of the mobile elements during bauxitization are alkaline and alkaline earth elements that do not form secondary minerals and are generally depleted in the profile.

In addition to correlation between Fe and Al ($R^2 = 0.6164$, Figure 8), these elements presented good correlation with Sc, V and P, confirming the opposite tendency of enrichment of high potential ionic elements during weathering. The HREE also showed significant correlations with Fe indicating that these elements may be precipitated in the Fe oxy-hydroxides. Liu et al. (2018) and Mondillo et al. (2019) claims that HREE could show a greater affinity for Fe oxide than LREE.

The four factors obtained from factor analysis reflected the intense weathering that the studied area has experienced. The first factor seems to indicate areas with greater and lesser advance of the lateritic process (positive and negative loadings, respectively), with the last one indicating a greater occurrence of unweathered primary minerals. During the pedogenic evolution, the chemical elements of low ionic potential, such as alkaline and earth alkaline, tend to be gradually released with destabilization of primary mineralogy of parent rocks. Thus, its presence in the stream sediment samples must be reflecting the primary mineralogy of less weathered rocks partially outcropping in the region.

Meanwhile, the second factor showed Si leaching of the weathering profile and relative enrichment of Al and Fe. These last two elements tend to form insoluble oxides and hydroxides remaining in the top of the profile, usually related to Nb, Th, P, V, Ti and REE (Goldschmidt 1937; Ahmadnejad et al. 2017; Ellahi et al. 2017).

The third and the fourth factors showed the distribution of REE in the region, with LREE widely distributed in the area while the HREE occurred more consistently in the northern and central portion. These are also the areas with the highest contents of Fe, supporting the behavior found in the univariate analysis. The relative enrichment of elements with high ionic

potential and less mobility in the surface environment, such as REE, is well documented (e.g. Ce content up to 399 ppm). According to Cocker (2014), these elements are found in a variety of primary minerals, and when the breakdown of the structure through weathering occurs, they are released as ions in solution. These ions can be adsorbed on clays or be fitted in the Fe and Mn oxy-hydroxides or participate in the composition of secondary minerals. Any of these mineral phases may be carried by drainages and could contribute to the chemical composition of stream sediments in a given catchment.

The HFSE occurred in the fourth factor. These elements tend to be immobile during metamorphism and weathering, and are indicative of the presence of primary minerals, such as apatite, amphiboles and zircon, reflecting the maturity of the weathering processes (Lapworth et al. 2012). Nevertheless, Melfi et al. (1996) observed high mobility of Zr, Ti and Nb during bauxitization. Another element association observed in the first factor is P-Ba-Sr-Mg-Ca. That could be related to the presence of phosphates such as apatite in the bedrock of the region.

5.2. Genesis of the lateritic profile

At the ITJ, the SiO_2 content decreases as we move from bottom to top in the profile (Figure 12), while the Al_2O_3 increases in the same direction. The Na_2O and K_2O are completely leached above horizon (iii), while the Fe_2O_3 content appears to increase to a maximum in this, decreases in the horizon (iv) and increases again at the horizon (v). Considering the typical weathering regolith from Anand and Paine (2002), the horizon (i) is related to the bedrock whereas horizon (ii) is the saprock. Horizon (iii) is interpreted as the saprolite, since some textural characteristics of the rock substratum are present.

The chemical index of alteration (CIA) from Nesbitt and Young (1982) reflects the breakdown of feldspars to kaolinite (McQueen 2006). The CIA continuous increase from the bedrock to the saprock (between 58 and 71) is well documented on the ITJ profile (Figure 12) and may be interpreted as the weathering front. The breakdown of K-feldspar into kaolinite starts at the weathering front and continuously intensifies towards the saprolite. Another reaction at the weathering front, which was not directly observed but can be deduced, is the transformation of biotite and amphibole into goethite. In the saprolite, the presence of the halloysite may indicate that, at least locally, the K-feldspar was initially transformed

into halloysite, before it turned into kaolinite (Anand et al. 1985). The dickite, locally present in the saprolite, is a kaolinite polymorph (Bailey 1963) and it is probably also a result of the K-feldspar breakdown. The Figure 19 presents bivariate plots considering the results from the samples of ITJ, CDF and VLT. The negative correlation ($R^2 = 0.9685$) between Al_2O_3 and SiO_2 (Figure 19A) supports the lateritic evolution, and the positive correlation ($R^2 = 0.2204$) between Al_2O_3 and Fe_2O_3 (Figure 19B) suggest that they behaved as immobile pairs during the weathering process. The loss on ignition (LOI) may be used as an indirect indication of gibbsite, kaolinite, and goethite (Anand and Paine 2002), and this is highlighted by the significant positive correlation ($R^2 = 0.9829$) between Al_2O_3 and LOI (Figure 19C), besides the petrographic evidence of the breakdown of the K-feldspar into kaolinite. The petrographic evidence suggesting the evolution of the association of amphibole and biotite in the bedrock, to goethite in the pedolith have some support by the positive correlation ($R^2 = 0.2630$) between Fe_2O_3 and LOI (Figure 19D).

The horizons (iv) and (v) may be related to the pedolith and lateritic duricrust from the Anand and Paine (2002) model. On the other hand, the conglomerate-like texture of the bauxite blocks are not common in the considered model. Another important characteristic is that ITJ profile is located in the bottom of a hill slope, in an area with high slopes angles. Thus, these features could suggest that these horizons were deposited through surficial sedimentation processes. Nevertheless, the positive correlation between the pairs (Figure 19-E-F) Yb-Lu ($R^2 = 0.9569$) and Nb-Ta ($R^2 = 0.6611$) indicates that these samples are genetically related (MacLean and Barret 1993; Sidbe and Yalcin 2018). Therefore, the bauxites may be classified as sedimentary (Bogatyrev et al. 2009), and since the profile that contains the mineralization retains some characteristics of the bedrock, it is probably a result of a proximal deposition (Haniłçi 2013; Sidbe and Yalcin 2018). The main reaction, in terms of the mineralization, happened between the saprolite and the pedolith, which was the pseudomorphic replacement of feldspars by gibbsite. The nordstrandite is commonly related to bauxitic environments in which the bedrock is composed of carbonate rocks, but it may also be the product of the weathering of alkali igneous rocks (Kovacs-Palfy et al. 2008). On the other hand, the experiments from Barnhisel and Rich (1965) showed that gibbsite is better crystallized in acid environments, whereas nordstrandite better crystallizes in slightly acid to neutral, or acid conditions in systems with relatively low amounts of Na and Cl. In addition, Schoen and Roberson (1970) showed that nordstrandite forms from bayerite, which was not observed here, during aging at intermediate to high pH values. Thus, the presence of the nordstrandite in CDF could be related to local conditions of weathering, and/or to the bedrock geochemical composition in the region, which was not directly observed in this study.

Considering the ternary diagram (Figure 20) of laterites classification from Aleva and Creutzberg (1994), the samples of the bedrock and saprock were classified as kaolin and bauxitious kaolin respectively, while the samples of the saprolite were classified as bauxitious kaolin, but also reached the bauxitic laterite region. The bauxite blocks were placed mainly in the siliceous bauxite field, but also reached the bauxitic region.

5.3. High Field Strength Elements

The positive correlation of Zr with Hf ($R^2 = 0.9454$), Nb ($R^2 = 0.7122$) and Ta ($R^2 = 0.4665$), observed throughout all weathered profile (Figure 21A-C), suggests that these HFSE may be related to zircon, which is the most stable mineral in response to weathering (Goldich 1938; Pidgeon et al. 2019). On the other hand, the Th ($R^2 = 0.1251$) and W ($R^2 = 0.0004$) showed no correlation with Zr, and thus, these two HFSE contents are probably not related to zircon (Figure 21D-E).

There is no obvious interpretation for the behavior of W, which usually increases upwards (Anand and Paine 2002), but in this case, it was leached from the profile. The Th presented the greatest increment upwards the profile. The composition of the chevkinite group is closely approached by the formula $A_4BC_2D_2Si_4O_{22}$, where usually A = REE, Ca, Sr, Th; B = Fe^{2+} ; C = Fe^{+3} , Fe^{+2} , Mn, Mg, Zr, Nb; D = Ti (Baginski and MacDonald 2013). Since Fernandes et al. (2019) identified the minerals of the chevkinite group, it is reasonable to suggest that at least part of the Th content in the pedolith may have been derived from the weathering of the rocks of the Volta do Rio Plutonic Suite. The Th is often adsorbed or incorporated by the iron hydroxides and can be present in Ti-phases minerals (Braun et al. 1993; Gamaletsos et al. 2011), and since this mineralogy is observed in the profile it is also a possibility to be considered.

5.4. Rare Earth Elements

There are four main REE modes of occurrence related to sedimentary bauxites: (i) the replacement of ions with similar size in aluminosilicate minerals; (ii) adsorption of the REE particle on the clay minerals surface; (iii) precipitation of secondary mineral during weathering and; (iv) contained in the detrital minerals (Takahashi et al. 2000; Laveuf and Cornu 2009; Zamanian et al. 2016; Wang et al. 2018; Ling et al. 2018). The phosphates typically display REE content that is economically explored, and they are commonly enriched in LREE when compared to HREE (Balaram 2019). Therefore, the phosphate weathering is expected to release important REE quantities and, even small amounts of phosphates, and it may largely influence the REE signature and budget of soils (Aide and Pavich 2002; Galán et al. 2007). The secondary Fe hydroxides and oxides, as well as Mn-oxides, together with zircon and Ti-phases minerals are important HREE scavengers (Haniłçi 2013; Liu et al. 2018).

Considering that the ITJ lateritic profile is of the sedimentary type, the discussions about REE in terms of the vertical column should be avoided, because it would be necessary several assumptions, since the surficial processes could remove key horizons to understand the pedogenic evolution (Bogatyrev et al. 2009; Zamanian et al. 2016). On the other hand, the positive correlation between the pairs Yb-Lu and Nb-Ta, indicates that these samples are genetically related and thus, some inferences can be made about the REE-bearing minerals.

The positive correlation between (Figure 22A-C) P and the total of REE ($R^2 = 0.5422$), HREE ($R^2 = 0.5940$) and LREE ($R^2 = 0.5337$), leads to the interpretation that apatite, an accessory mineral which is observed in the bedrock, should be one of the candidates to be the REE-bearing parent mineral, together with those of the chevkinite group that Fernandes et al. (2019) identified. The positive correlation between (Figure 22D-E)

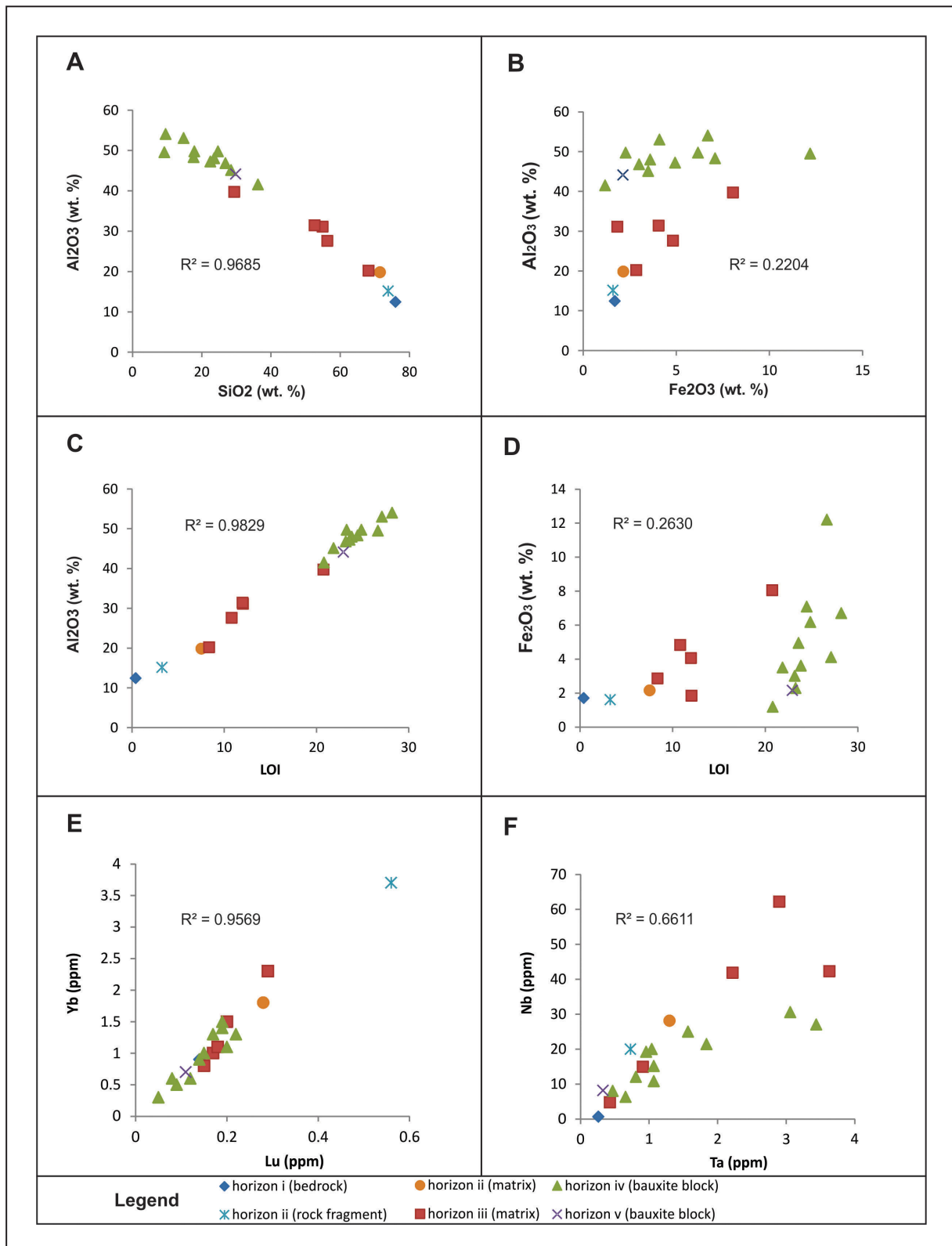


FIGURE 19. Selected bivariate plots showing the correlation between Al_2O_3 with: SiO_2 (A), Fe_2O_3 (B), LOI (C). Bivariate plot with correlation between Fe_2O_3 with LOI (D). Bivariate plots with correlation between Yb with Lu (E) and Nb with Ta (F).

HREE with both Zr ($R^2 = 0.4167$) and Ti ($R^2 = 0.3233$) suggests that zircon and titanite, which are minerals that are spatially related with the bauxite mineralization, could hosts HREE content. If some advanced study (e.g. in-situ laser ablation-inductively coupled plasma mass spectrometric analyses) confirms the presence of HREE, or anyone of the REE + Sc +

Y, in these resistate minerals, an opportunity is opened for the recovery of the REE as by-product of bauxite mining. These resistate solid phases remain unaffected by the Bayer process (Hind et al. 1999), which could be furthered accessed in the bauxite residue, and thus, a new process of the REE + Sc + Y recovery may be started (Vind et al. 2018; Mondillo et al. 2019).

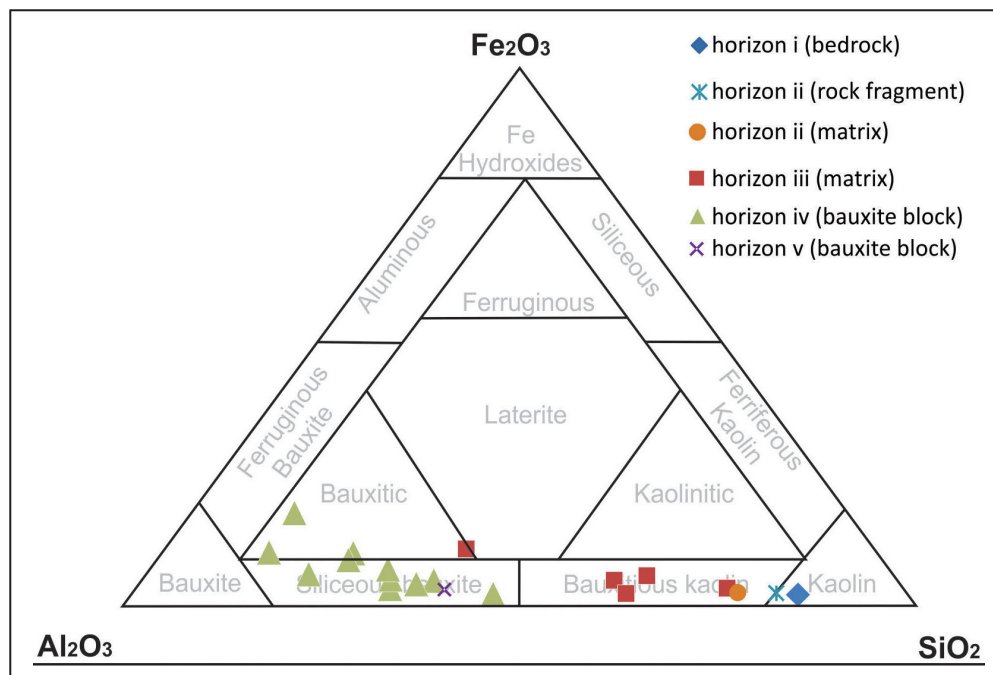


FIGURE 20. (A) Ternary diagram of the laterites classification according to Aleva and Creutzberg (1994).

There is no common sense in terms of the mobility of the REE during pedogenic evolution. Some author defends that REE show low mobility and fractionation (Karadag et al. 2009 and references therein), while others that REE show mobility during several stages of the bauxitization process (Zamanian et al. 2016 and references therein). In addition, the LREE and the HREE distribution may be direct reflection of the stability of the REE carrier complex (Yuste et al. 2017; Ahmadnejad et al. 2017)

The La/Yb ratio showed a fractionation between LREE and HREE, highlighting a relative LREE enrichment and depletion of the HREE. We did not identify any REE carrier complex such as fluorocarbonate, but this could be a matter of sampling and further works should be alert to the possibility of REE-carbonate complex existence.

The occurrence of positive Ce anomalies is usually related to the oxidation of Ce (III) to Ce (IV), followed by the preferential incorporation of Ce by Fe and Mn oxides and/or hydroxides (Takahashi et al. 2000; Laveuf and Cornu 2009). In addition, the Ce can also be present as REE-carbonate complexes (Yuste et al. 2017). On the other hand, Braun et al. (1990) showed that this is not always the case, and that positive Ce anomalies also develop in the non-ferruginous horizons and may, or may not, precipitate cerianite. According to these authors, there are two main options for the REE that remain in the soil, which are to take part in formation of other REE-bearing minerals or to be adsorbed on clay surfaces. The cerianite or any other REE-bearing mineral or carbonate complex was not identified by petrography or XRD analysis, and thus it is reasonable to suggest that adsorption may be the process that is responsible for the Ce content, and consequently for the pronounced positive Ce anomalies.

5.5. Insights on the Jequié Complex bauxite mineral system

The controls on the formation of bauxite deposits include bedrock lithology, mechanisms of chemical weathering,

influence of geomorphology and climatic and/or paleoclimatic conditions (Freyssinet et al. 2005; Bogatyrev et al. 2009), may be interpreted as the critical processes in terms of mineral system concept (Wyborn et al. 1994; McCuaig and Hronsky 2014).

Granitic rocks constitute the parent materials of many significant bauxite deposits, and the process of Al enrichment is mostly controlled by the rate of weathering, rather than of the initial Al content (Freyssinet et al. 2005). Additionally, residual deposits resulting from the weathering of plutonic rocks with phosphates are favorable to show REE-bearing mineralization (Balaram 2019). Both critical processes previously mentioned can be deduced in the bedrock of the Volta do Rio Plutonic Suite.

The physicochemical mechanisms of weathering were not within the objective of this work, but some considerations may be placed. The lateritic weathering can proceed with pH varying between 3.9 and 9, with the removal of CNK components happening with pH lower than 5, and Al precipitation with pH varying between 5 and 8.5 (Bogatyrev et al. 2009). The leaching of CNK components and Si is well documented on the ITJ profile, while the presence of the nordstrandite on CDF is a clue for the local changes that the pH has showed during the Al precipitation.

Considering the influence of geomorphology, most of the bauxite deposits are present on ancient lateritic planation surfaces (Aleva and Creutzberg 1994). The Serras Marginais do Leste da Bahia, which is the geomorphologic unit that hosts the bauxite mineralization, is mainly constituted by residual ridges related to the Gondwana planation surface of the late-cretaceous period (Silva 2009) with extremely dissected slopes. The late-cretaceous is a period of a well-documented bauxite deposits formation (Freyssinet et al. 2005). Chardon et al. (2006) showed that the bauxite occurrences of the West African rifted margin are probably related to the presence of two Meso-Cenozoic planation surfaces and suggest the hypothesis of a symmetric morphotectonic and morphoclimatic evolution with respect to

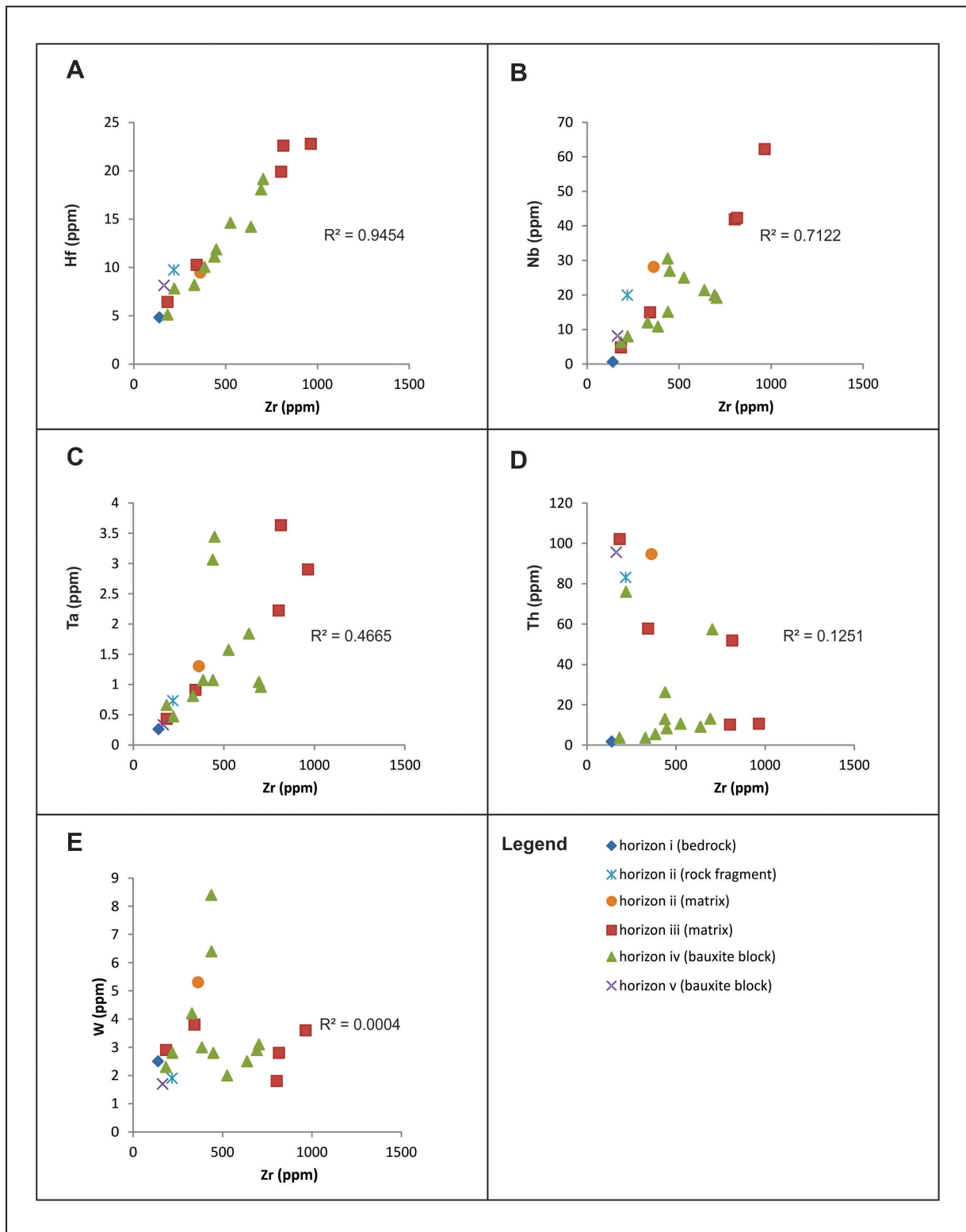


FIGURE 21. Selected bivariate plots showing the correlation between Zr and: Hf (A), Nb (B), Ta (C), Th (D) and W (E).

the Atlantic margin. Therefore, we suggest that future studies, including the goethite dating with [(U-Th)]/He method and the $^{40}\text{Ar}/^{39}\text{Ar}$ dating of k-bearing weathering minerals (e.g. Ansart et al. 2022), should be carried out in order to test this hypothesis. At Brazil southeastern region, in the Mantiqueira Province, there are bauxite deposits and occurrences with several similar characteristics of this study (Costa 2016). The bedrock of the Cataguazes bauxite deposit is composed of granulitic rocks of

magmatic origin. The landscape evolution happened during the Gondwana planation surface and the allochthonous bauxite occurs in the basis of the hills slope (Beissner et al. 1997). At Mirai deposit, the bedrocks are composed of granulitic rocks and the bauxites occur like massive angular fragments in the hill slopes, partially maintaining the structures of the parent rock (Lopes and Carvalho 1990). Soares et al. (2014) presents an occurrence of bauxite at the Caparaó Suite. The mineralization

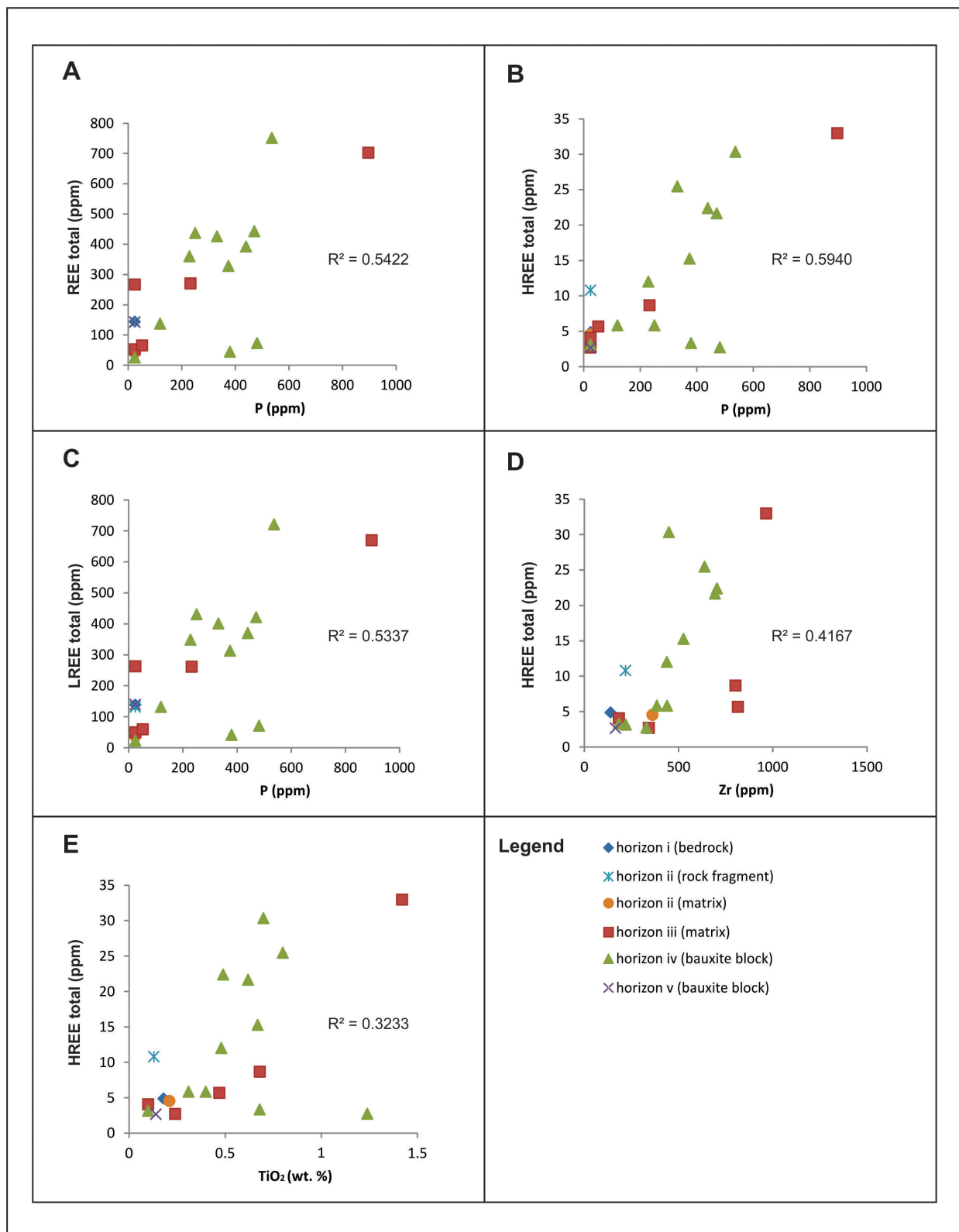


FIGURE 22. Selected bivariate plots showing the correlation between P and: total of REE (A), HREE (B) and LREE (C). Bivariate plots showing correlation between HREE with Zr (D) and TiO₂ (E).

was developed over charnockitic rocks and placed in the half slopes hills.

The lateritic index (LI) from Iza et al. (2020) was developed to analyze the relationship between weathering and gamma-spectrometric data. The areas with high LI present greater probability to have lateritic duricrusts. The areas with high

index showed a good spatial correlation with the Serras Marginais do Leste da Bahia and thus, could be an interesting tool for mineral exploration focused on bauxite.

The climatic conditions that favor the bauxitization process highlighted an average annual temperature exceeding 22 °C, with an annual rainfall distributed over nine to eleven months

(Aleva and Creutzberg 1994). Deposits such as of this study, that are placed in areas with no currently favorable climatic conditions can be interpreted as simply fossils of more favorable paleoclimatic conditions (Freyssinet et al. 2005).

6. Conclusions

The Jequié Block is located in the northeastern portion of the São Francisco Craton and it is characterized by cogenetic, enderbite-charnockite plutons, which were intruded by gabbros, norites and anorthosites, and subsequently all these rocks were re-equilibrated in granulite facies. Three bauxite occurrences were mapped in the southeastern portion of the Jequié Block, named Itaji (ITJ), Casa de Farinha (CDF) and Valentim (VLT). It can be concluded that:

The stream sediment geochemical maps for the major elements indicate the increased presence of Al, Fe, REE+Y+Sc and Ce in the catchments in the region where bauxite mineralization occurs;

The horizons of the ITJ vertical profile indicate a lateritic sequence consisting of, from bottom to top, bedrock (i), saprock (ii), saprolite (iii), pedolith (iv) and lateritic duricrust (v);

The lateritic sequence is of the sedimentary type, with proximal deposition.

Acknowledgements

This paper was funded by the Contendas-Macajuba Project, CC. 4116.084. The authors would like to thank Dr. Débora Correia Rios, head of the Laboratory of Mineral Technology - X Ray, and Tâmara Vieira Reis, laboratory technician, that provided enormous help during the acquisition and interpretation of XRD data. DAM would like to thank Eduardo Moussalle Grissolia for the help with the mass balance research, and Rodrigo Soares dos Santos Vieira, for his contribution with the SRTM data and the Slope Map. The authors are grateful to the editors and the reviewers of the JGSB for the comments that were essential to improve the manuscript quality.

Authorship credits

Author	A	B	C	D	E	F
DAM						
CCS						
FPS						
ARASM						
CMSC						
RCLMO						
ILIEH						

A - Study design/Conceptualization B - Investigation/Data acquisition
 C - Data Interpretation/ Validation D - Writing
 E - Review/Editing F - Supervision/Project administration

References

Ahmadnejad F., Zamanian H., Taghipour B. Zarasvandi A., Buccione R., Ellahi S.S. 2017. Mineralogical and geochemical evolution of the Bidgol bauxite deposit, Zagros Mountain Belt, Iran: implications for ore genesis, rare earth elements fractionation and parental affinity. *Ore Geology Reviews*, 86, 755- 783. <https://doi.org/10.1016/j.oregeorev.2017.04.006>

- Aide M.T., Pavich Z. 2002. Rare earth element mobilization and migration in a Wisconsin spodosol. *Soil Science*, 167(10), 680-691. <http://dx.doi.org/10.1097/00010694-200210000-00006>
- Aleva G.J.J., Creutzberg D. 1994. Laterites: concepts, geology, morphology and chemistry. Wageningen, ISRIC, 169 p.
- Almeida F.F.M. 1977. O Cráton do São Francisco. *Revista Brasileira de Geociências*, 7(4), 349-364. <https://doi.org/10.25249/0375-7536.1977349364>
- Alvares C.A., Stape J.L., Sentelhas C.P., Gonçalves J.L.M., Sparovek G. 2013. Köppen's climate classification map for Brazil. *Meteorologische Zeitschrift*, 22(6), 711-728. <https://doi.org/10.1127/0941-2948/2013/0507>
- Anand R.R., Gilkes R.J., Armitage T.M., Hillyer J.W. 1985. Feldspar weathering in lateritic saprolite. *Clays and Clay Minerals*, 33, 31-43. <https://doi.org/10.1346/CCMN.1985.0330104>
- Anand R.R., Paine M. 2002. Regolith geology of the Yilgarn Craton, Western Australia: implications for exploration. *Australian Journal of Earth Sciences*, 49(1), 3-162. <http://dx.doi.org/10.1046/j.1440-0952.2002.00912.x>
- Ansart C., Quantin C., Calmels D., Allard T., Roig J.Y., Coueffe R., Heller B., Pinna-Jamme R., Nouet J., Reguer S., Vantelon D., Gautheron C. 2022. (U-Th)/He Geochronology Constraints on Lateritic Duricrust Formation on the Guiana Shield. *Frontiers in Earth Science*, 10, 1-19. <https://doi.org/10.3389/feart.2022.888993>
- Bailey S.W. 1963. Polymorphism of the kaolin minerals. *The American Mineralogist*, 48, 1196-1209.
- Baginski B., MacDonald R. 2013. The chevkinite group: underestimated accessory phases from a wide range of parageneses. *Mineralogia*, 44(3-4), 99-114. <https://doi.org/10.2478/mipo-2013-0006>
- Balaram V. 2019. Rare earth elements: a review of applications, occurrence, exploration, analysis, recycling, and environmental impact. *Geoscience Frontiers*, 10(4), 1285-1303. <https://doi.org/10.1016/j.gsf.2018.12.005>
- Barbosa J.S.F. 1990. The granulites of the Jequié Complex and Atlantic Coast Mobile Belt, Southern Bahia, Brazil - an expression of Archean/Early Proterozoic Plate Convergence. In: Vielzeuf D., Vidal P. (eds.). *Granulites and crustal evolution*. Springer. p. 195-221. https://doi.org/10.1007/978-94-009-2055-2_11
- Barbosa J.S.F., Sabaté P. 2002. Geological features and the Paleoproterozoic collision of four Archean crustal segments of the São Francisco Craton, Bahia, Brazil: a synthesis. *Anais da Academia Brasileira de Ciências*, 74(2), 343-359. <https://doi.org/10.1590/S0001-37652002000200009>
- Barbosa J.S.F., Sabaté P. 2004. Archean and Paleoproterozoic crust of the São Francisco Craton, Bahia, Brazil: geodynamic features. *Precambrian Research*, 133(1-2), 1-27. <https://doi.org/10.1016/j.precamres.2004.03.001>
- Barbosa J.S.F., Cruz S.C.P., Souza J.S.S. 2012. Terrenos metamórficos do embasamento. In: Barbosa J.S.F. (ed.). *Geologia da Bahia: pesquisa e atualização*. Salvador, Companhia Baiana de Pesquisa Mineral. p. 101-202. <http://www.cbpm.ba.gov.br/book/geologia-da-bahia-pesquisa-e-atualizacao/>
- Barnhisel R.I., Rich C.I. 1965. Gibbsite, Bayerite, and Nordstrandite Foration as affected by Anions, pH, and mineral surfaces. *Soil Science Society of America Journal*, 29, 531-534. <https://doi.org/10.2136/sssaj1965.03615995002900050018x>
- Beissner H., Carvalho A., Lopes L.M., Valetton I. 1997. The Cataguazes bauxite deposit. In: Carvalho A., Boulangé B., Melfi A.J., Lucas Y. (eds.). *Brazilian bauxites*. São Paulo, Universidade de São Paulo. p. 195-208.
- Bogatyrev B.A., Zhukov V.V., Tsekhovskiy Y.G. 2009. Formation conditions and regularities of the distribution of large and superlarge bauxite deposits. *Lithology and Mineral Resources*, 44, 135-151. <https://doi.org/10.1134/S0024490209020035>
- Braun J.J., Pagel M., Muller J.P., Bilong P., Michard A., Guillet B. 1990. Cerium anomalies in lateritic profiles. *Geochimica et Cosmochimica Acta*, 54(3), 781-795. [https://doi.org/10.1016/0016-7037\(90\)90373-S](https://doi.org/10.1016/0016-7037(90)90373-S)
- Braun J.J., Pagel M., Herbillon A., Rosin C. 1993. Mobilization and redistribution of REES and thorium in a syenitic lateritic profile: a mass balance study. *Geochimica et Cosmochimica Acta*, 57(18), 4419-4434. [https://doi.org/10.1016/0016-7037\(93\)90492-F](https://doi.org/10.1016/0016-7037(93)90492-F)
- Chardon D., Chevillotte V., Beauvis A., Grandin G., Boulangé B. 2006. Planation, bauxites and epeirogeny: one or two paleosurfaces on the West African margin? *Geomorphology*, 82(3-4), 273-282. <https://doi.org/10.1016/j.geomorph.2006.05.008>

- Cocker M.D. 2014. Lateritic, supergene rare earth element (REE) deposits. In: Forum on the Geology of Industrial Minerals, 48. Arizona Geological Survey Special Paper #9, 1-18. Available online at: <http://hdl.handle.net/10150/629374> / (accessed on 12 April 2022).
- Costa M.L. 2016. Alumínio e bauxita no Brasil. In: Melfi A.J., Misi A., Campos D.A., Cordani U.G. (Eds). Recursos minerais no Brasil: problemas e desafios. Rio de Janeiro, Academia Brasileira de Ciências. p. 166-173. Available online at: <https://www.abc.org.br/2013/09/05/recursos-minerais-no-brasil-problemas-e-desafios/> / (accessed on 12 April 2022).
- Ellahi S.S., Taghipour B., Nejadhadad M. 2017. The role of organic matter in the Formation of High-Grade Al Deposits of the Dopolan Karst Type Bauxite, Iran: mineralogy, geochemistry, and sulfur isotope data. Minerals, 7(6), 97. <https://doi.org/10.3390/min7060097>
- Farr T.G., Rosen P.A., Caro E., Crippen R., Duren R., Hensley S., Kobrick M., Paller M., Rodriguez E., Roth L., Seal D., Shaffer S., Shimada J., Umland J., Werner M., Oskin M., Burbank D., Alsdorf D. 2007. The Shuttle Radar Topography Mission. Reviews of Geophysics, 45, 1-33. <https://doi.org/10.1029/2005RG000183>
- Fernandes P.C.D. 1996. Projeto Terras Raras no Complexo Jequié, Bahia. Relatórios internos. Salvador, CPRM, 11 p. Available online at: <https://rigeo.cprm.gov.br/handle/doc/14321> / (accessed on 19 July 2021).
- Fernandes P.C.D., Frantz J.C., Rios D.C., Davis D.W., Porcher C.C., Conceição R.V., Coelho R.E. 2019. The Jequié Complex revisited: A U-Pb geochronological reappraisal of the geology and stratigraphy of the Jequié-Itagi Area (Bahia, Brazil). Anuário do Instituto de Geociências, 42, 166-178. https://doi.org/10.11137/2019_1_166_178
- Filzmoser P., Hron K., Reinman C. 2009. Univariate statistical analysis of environmental (compositional) data: problems and possibilities. Science of The Total Environment, 407(23), 6100-6108. <https://doi.org/10.1016/j.scitotenv.2009.08.008>
- Freyssinet Ph., Butt C.R.M., Morris R.C., Piantone P. 2005. Ore-Forming processes related to Lateritic Weathering. Economic Geology, 100th Anniversary Volume, 681-722. <https://doi.org/10.5382/AV100.21>
- Galán E., Caliani-Fernández J.C., Miras A., Aparicio P., Márquez M.G. 2007. Residence and fractionation of rare earth elements during kaolinization of alkaline peraluminous granites in NW Spain. Clay Minerals, 42(3), 341-352. <http://dx.doi.org/10.1180/claymin.2007.042.3.07>
- Goldich S.S. 1938. A study in rock-weathering. Journal of Geology, 46(1), 17-58. <https://doi.org/10.1086/624619>
- Goldschmidt V.N. 1937. The principles and distribution of chemical elements in minerals and rocks. Journal of the Chemical Society, 0, 655-673. <https://doi.org/10.1039/JR9370000655>
- Gamaletsos P., Godelitsas A., Mertzimekis T.J., Gottlicher J., Steininger R., Xanthos S., Berndt J., Klemme S., Kuzmin A., Bárdossy G. 2011. Thorium partitioning in Greek industrial bauxite investigated by synchrotron radiation and laser-ablation techniques. Nuclear Instruments in Physics Research Section B: Beam Interactions with Materials and Atoms, 269(24), 3067-3073. <https://doi.org/10.1016/j.nimb.2011.04.061>
- Haniilçi N. 2013. Geological and geochemical evolution of the Bilkardagi bauxite deposits, Karaman, Turkey: transformation from shale to bauxite. Journal of Geochemical Exploration, 133, 118-137. <https://doi.org/10.1016/j.gexplo.2013.04.004>
- Hind A.R., Bhargava S.K., Grocott S.C. 1998. The surface chemistry of Bayer process solids: a review. Colloids and Surfaces A: Physicochemical and Engineering Aspects, 146(1-3), 359-374. [https://doi.org/10.1016/S0927-7757\(98\)00798-5](https://doi.org/10.1016/S0927-7757(98)00798-5)
- IBGE. 2019. Biomas brasileiros (1:250.000). Available online at: <https://www.ibge.gov.br/geociencias/informacoes-ambientais/15842-biomas.html?=&t=acesso-ao-produto> / (accessed on 14 August 2021).
- IBGE. 2021. BDIA - Banco de Dados de Informações Ambientais – Geomorfologia. Available online at: <https://bdiaweb.ibge.gov.br/#/home> / (accessed on 20 August 2021).
- INEMA. 2019. Mapeamento de Cobertura Vegetal do Estado da Bahia, na escala 1:50.000. Available online at: <http://mapa.geobahia.ba.gov.br/> / (accessed on 14 September 2021).
- Iza E.R.H.F., Santos R.S.V., Cruz Filho B.E. 2020. Integration of multisource data to support the identification of lateritic regolith in Eastern - Bahia, northeastern Brazil. Journal of the Geological Survey of Brazil, 3(1), 1-24. <https://doi.org/10.29396/jgsb.2020.v3.n1.1>
- Karadag M.M., Küpeli S., Arýk F., Ayhan A., Zedef V., Döylen A. 2009. Rare earth element (REE) geochemistry and genetic implications of the Mortas bauxite deposit (Seydisehir/Konya-Southern Turkey). Geochemistry: Chemie der Erde, 69(2), 143-159. <https://doi.org/10.1016/j.chemer.2008.04.005>
- Kovacs-Palfy P., Velledits F., Konya P., Foldvari M., Solymos K.G. 2008. Nordstrandite – A new occurrence from Hungary. Acta Mineralogica-Petrographica, 48, 43-48. Available online at: <http://acta.bibl.u-szeged.hu/id/eprint/25151>
- Lapworth D.J., Knights K.V., Key R.M., Johnson C.C., Ayoade E., Adekanmi M.A., Arisekola T.M., Okunlola O.A., Backman B., Eklund M., Everett P.A., Lister R.T., Ridgway J., Watts M.J., Kemp S.J., Pitfield P.E.J. 2012. Geochemical mapping using stream sediments in west-central Nigeria: Implications for environmental studies and mineral exploration in West Africa. Applied Geochemistry, 27(6), 1035-1052. <https://doi.org/10.1016/j.apgeochem.2012.02.023>
- Laveuf C., Cornu S. 2009. A review in the potentiality of the Rare Earth Elements to trace pedogenetic processes. Geoderma, 154(1-2), 1-12. <https://doi.org/10.1016/j.geoderma.2009.10.002>
- Ling K.Y., Zhu X.Q., Tang H.S., Du S.J., Gu J. 2018. Geology and geochemistry of the Xiaoshanba bauxite deposit, Central Guizhou Province, SW China: implications for the behavior of trace and rare earth elements. Journal of Geochemical Exploration, 190, 170-186. <https://doi.org/10.1016/j.gexplo.2018.03.007>
- Liu Y., Cheng Q., Zhou K., Xia Q., Wang X. 2016. Multivariate analysis for geochemical process identification using stream sediment geochemical data: a perspective from compositional data. Geochemical Journal, 50(4), 293-314. <http://dx.doi.org/10.2343/geochemj.2.0415>
- Liu H., Pourret O., Guo H., Martinez R.E., Zouhri L. 2018. Impact of hydrous manganese and ferric oxides on the behavior of aqueous Rare Earth Elements (REE): evidence from a modeling approach and implication for the sink of REE. International Journal of Environmental Research and Public Health, 15, 2837. <https://doi.org/10.3390/ijerph15122837>
- Lopes M.L., Carvalho A. 1990. Gênese da Bauxita de Miari, MG. Revista Brasileira de Geociências, 19(4), 462-469. Available online at: <https://papego.igc.usp.br/index.php/rbg/article/view/10354/9739>
- MacLean W.H., Barret T.J. 1993. Lithochemical techniques using immobile elements. Journal of Geochemical Exploration, 48(2), 109-133. [https://doi.org/10.1016/0375-6742\(93\)90002-4](https://doi.org/10.1016/0375-6742(93)90002-4)
- Marinho M.M., Sabaté P., Barbosa J.S.F. 1995. The Contendas-Mirante volcano-sedimentary belt. Boletim IG-USP, Publicação Especial, 17, 37-72. <https://doi.org/10.11606/issn.2317-8078.v0i17p38-72>
- McCuaig T.C., Hronsky J.M.A. 2014. The mineral system concept: the key to exploration targeting. In: Kelley K.D., Golden H.C. Building exploration capability for the 21st Century. Society of Economic Geologists, Special Publications 18, 153-176. <https://doi.org/10.5382/SP18.08>
- McQueen K.G. 2006. Unravelling the regolith with geochemistry. In: Fitzpatrick R.W., Shand P. (eds.). Regolith 2006: Consolidation and dispersion of ideas. CRC LEME. p. 230-235. Available online at: <https://www.researchgate.net/publication/242255710> / (accessed on 25 November 2021).
- Melfi A.J., Subies F., Nahon D., Formoso M.L.L. 1996. Zirconium mobility in bauxites of Southern Brazil. Journal of South American Earth Sciences, 9(3-4), p. 161-170. [https://doi.org/10.1016/0895-9811\(96\)00003-X](https://doi.org/10.1016/0895-9811(96)00003-X)
- Mondillo N., Balassone G., Boni M., Chelle-Michou C., Cretella S., Mormone A., Putzolu F., Santoro L., Scognamiglio G., Tarallo M. 2019. Rare Earth Elements (REE) in Al- and Fe-(Oxy)-Hydroxides in Bauxites of Provence and Languedoc (Southern France): implications for the potential recovery of REEs as by-products of bauxite mining. Minerals, 9(9), 504. <https://doi.org/10.3390/min9090504>
- Mordberg L.E. 1996. Geochemistry of trace elements in Paleozoic bauxites profiles in northern Russia. Journal of Chemical Exploration, 57(1-3), 187-199. [https://doi.org/10.1016/S0375-6742\(96\)00036-2](https://doi.org/10.1016/S0375-6742(96)00036-2)
- Nesbitt H.W., Markovics G., Price R.C. 1980. Chemical processes affecting alkalis and alkaline earths during continental weathering. Geochimica et Cosmochimica Acta, 44(11), 1659-1666. [https://doi.org/10.1016/0016-7037\(80\)90218-5](https://doi.org/10.1016/0016-7037(80)90218-5)
- Nesbitt H.W., Young G.M. 1982. Early Proterozoic climates and plate motions inferred from major element chemistry of lutites. Nature, 299, 715-717. <http://dx.doi.org/10.1038/299715a0>
- Oliveira A.V. 2021. Resolução Nº 2, de 18 de junho de 2021. Diário Oficial da União. Brasília, Ministério de Minas e Energia/Secretaria de Geologia, Mineração e Transformação Mineral, Edição 115, Seção 1, 1 p. Available online at: <https://www.gov.br/imprensa nacional/pt-br/> / (accessed on 20 January 2022).
- Pidgeon R.T., Nemchin A.A., Roberts M.P., Whitehouse M.J., Bellucci J.J. 2019. The accumulation of non-formula elements in zircon

- during weathering: ancient zircons from the Jack Hills, Western Australia. *Chemical Geology*, 530, 119310. <https://doi.org/10.1016/j.chemgeo.2019.119310>
- Reimann C., Filzmoser P., Garret R.G. 2002. Factor analysis applied to regional geochemical data: problems and possibilities. *Applied Geochemistry*, 17(3), 185-206. [https://doi.org/10.1016/S0883-2927\(01\)00066-X](https://doi.org/10.1016/S0883-2927(01)00066-X)
- Retallack G.J. 2010. Laterization and bauxitization events. *Economic Geology*, 105(3), 655-667. <http://dx.doi.org/10.2113/gsecongeo.105.3.655>
- Rudnick R.L., Gao S. 2014. 4.1 - Composition of the Continental Crust. In: Holland H.D., Turekian K.K.B. (eds.), *Treatise on Geochemistry*. 2nd ed. Elsevier. p. 1-51. <https://doi.org/10.1016/B978-0-08-095975-7.00301-6>
- Santos F.P., Menezes R.C.L., Martins A.A.M., Pires A.S., Meirelles L.G.S., Lima E.G., Rodrigues T.R., Miranda D.A. 2020. Carta Geológica da Folha Manoel Vitorino SD.24-Y-B-I, Estado da Bahia, Escala 1:100.000. Programa Geologia, Mineração e Transformação Mineral, Salvador, CPRM. Available online at: <http://rigeo.cprm.gov.br/handle/doc/20473> / (accessed on 27 July 2021)
- Santos Junior G.R. Avaliação da variabilidade geoquímica de elementos terras raras, urânio e tório em perfis regolíticos/laterizados em rochas do Complexo Jequié Bahia, Brasil. Msc Dissertation, Instituto Federal de Educação Ciência e Tecnologia do Rio Grande do Norte, Natal, 109 p. Available online at: <http://memoria.ifrn.edu.br/handle/1044/1718> / (accessed on 16 August 2021)
- Schoen R., Roberson C.E. 1970. Structures of aluminum hydroxide and geochemical implications. *American Mineralogist*, 55(1-2), 43-77. Available online at: <https://pubs.geoscienceworld.org/msa/ammin/article-abstract/55/1-2/43/541198/Structures-of-aluminum-hydroxide-and-geochemical> / (accessed on 11 April 2023)
- Sidbe M., Yalcin M.G. 2018. Petrography, mineralogy, geochemistry and genesis of the Balaya bauxite deposits in Kindia region, Maritime Guinea, West Africa. *Journal of African Earth Geosciences*, 149, 348-366. <https://doi.org/10.1016/j.jafrearsci.2018.08.017>
- Silva T. M. 2009. Superfícies geomorfológicas do Planalto Sudeste Brasileiro: revisão teórico-conceitual. *Geo UERJ*, 20(20), p. 1-22. <http://dx.doi.org/10.12957/geouerj.2009.1426>
- Soares C.C.V., Varajão A.F.D.C., Varajão C.A.C., Boulangé B. 2014. Mineralogical, micromorphological and geochemical transformations in the initial steps of the weathering process of charnockite from the Caparaó Range, southeastern Brazil. *Journal of South American Earth Sciences*, 56, 30-40. <https://doi.org/10.1016/j.jsames.2014.08.005>
- Stausholm J. 2021. Rio Tinto releases fourth quarter production results. Published releases. London, Rio Tinto, 29 p. Available online at: <https://www.riotinto.com> / (accessed on 20 January 2022).
- Sun S.S., McDonough W.F. 1989. Chemical and isotopic systematics of oceanic basalts: implication for mantle composition and processes. In: Saunders A.D., Norry M.J. (eds.), *Magmatism in the Ocean Basins*, Geological Society Special Publication, 42, 313-345. <http://dx.doi.org/10.1144/GSL.SP.1989.042.01.19>
- Takahashi Y., Shimizu H., Usui A., Kagi H., Nomura M. 2000. Direct observation of tetravalent cerium in ferromanganese nodules and crusts by X-ray-absorption near-edge structure (XANES). *Geochimica et Cosmochimica Acta*, 64(17), 2929-2935. [https://doi.org/10.1016/S0016-7037\(00\)00403-8](https://doi.org/10.1016/S0016-7037(00)00403-8)
- Takehara L., Shintaku I., Rabelo D.M., Silveira F.V. 2015. Informe de Recursos Minerais, Série Minerais Estratégicos, n. 2. Programa Geologia do Brasil. Brasília, CPRM, 218 p. Available online at: <https://rigeo.cprm.gov.br/handle/doc/16923> / (accessed on 19 July 2021).
- Taylor S.R., McLennan S.M. 1985. *The Continental Crust: its composition and evolution*. Oxford, Blackwell Publishing, 328 p.
- Vind J., Malfliet A., Blanpain B., Tsakiridis P.E., Tkaczyk A.H., Vassiliadou V., Panias D. 2018, 8(2), 77. <https://doi.org/10.3390/min8020077>
- Wang W., Pranolo Y., Cheng C.Y. 2011. Metallurgical processes for scandium recovery from various resources: a review. *Hydrometallurgy*, 108(1-2), 100-108. <https://doi.org/10.1016/j.hydromet.2011.03.001>
- Wang R., Wang Q., Huang Y., Yang S., Liu X., Zhou Q. 2018. Combined tectonic and paleogeographic controls on the genesis of bauxite in the Early Carboniferous to Permian Central Yangtze Island. *Ore Geology Reviews*, 101, 468-480. <https://doi.org/10.1016/j.oregeorev.2018.07.013>
- Whitney D.L., Evans B.W. 2010. Abbreviations for names of rock-forming minerals. *American Mineralogist*, 95(1), 185-187. <http://dx.doi.org/10.2138/am.2010.3371>
- Wyborn L.A.I.; H, C.A.; Jaques A.L. 1994. Australian proterozoic mineral systems: essential ingredients and mappable criteria. In: Australian Institute of Mining and Metallurgy Annual Conference, p.109-115. Available online at: https://www.researchgate.net/publication/263884864_Australian_Proterozoic_mineral_systems_essential_ingredients_and_mappable_criteria / (accessed on 16 December 2021).
- Yuste A., Bauluz B., Mayayo M.J. 2017. Origin and geochemical evolution from ferrallitized clays to karst bauxite: An example from the Lower Cretaceous of NE Spain. *Ore Geology Reviews*, 84, 67-79. <https://doi.org/10.1016/j.oregeorev.2016.12.025>
- Zamanian H., Ahmadnejad F., Zarasvandi A. 2016. Mineralogical and geochemical investigations of the Mombi bauxitedeposit, Zagros Mountains, Iran. *Geochemistry Chemie der Erde*, 76(1), 13-37. <https://doi.org/10.1016/j.chemer.2015.10.001>